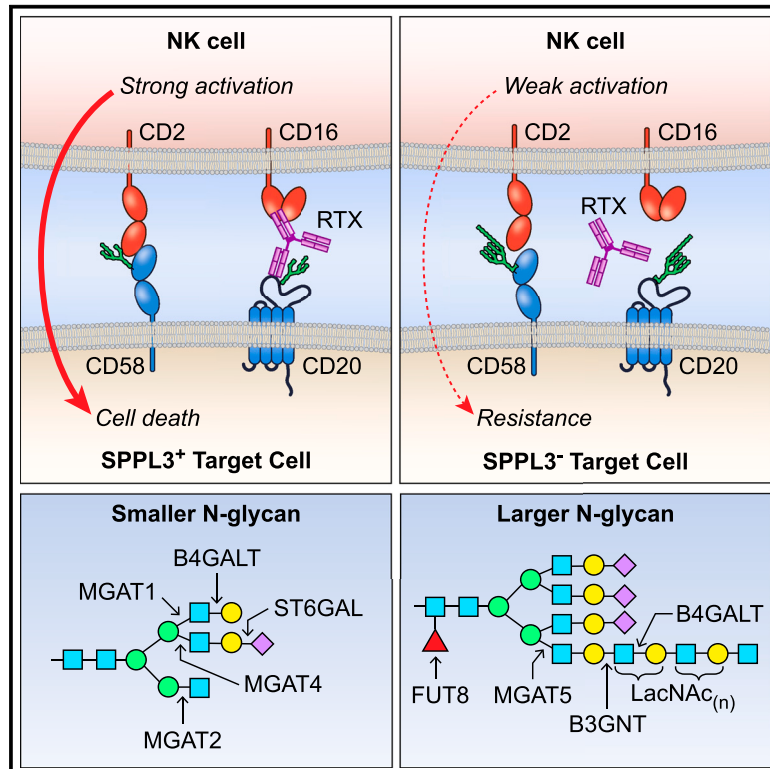# Functional genomics identifies *N*-acetyllactosamine extension of complex *N*-glycans as a mechanism to evade lysis by natural killer cells

Graphical abstract

Authors

Xiaoxuan Zhuang, James Woods, Yanlong Ji, ..., Louis M. Staudt, Kuan-Ting Pan, Eric O. Long

Correspondence

xiaoxuan.zhuang@nih.gov (X.Z.), elong@nih.gov (E.O.L.)

In brief

Somatic mutations drive cancer immune evasion. Zhuang et al. find *SPPL3* as crucial for sensitivity to NK-mediated killing. *SPPL3* deletion increases *N*-glycan complexity, which impairs NK receptor binding. *B3GNT2* is responsible for *N*-glycan extensions. Inhibition of this pathway restores cancer cell sensitivity, highlighting a potential strategy to improve cancer immunotherapy.

Highlights

- Deletion of *SPPL3* promotes resistance of malignant B cells to NK cell cytotoxicity

- Loss of *SPPL3* blocks ligand binding to NK receptors via increased *N*-glycosylation

- *B3GNT2* deletion reduces LacNAc addition and restores *SPPL3*-KO cell sensitivity to NK cells

- *SPPL3*-deficient cells are enriched in tetra-antennary *N*-glycans with LacNAc elongations

Cell Reports

Article

Functional genomics identifies *N*-acetyllactosamine extension of complex *N*-glycans as a mechanism to evade lysis by natural killer cells

Xiaoxuan Zhuang,[1,5,*] James Woods,[1] Yanlong Ji,[2,3,4] Sebastian Scheich,[5] Fei Mo,[6] Sumati Rajagopalan,[1] Zana A. Coulibaly,[5] Matthias Voss,[7] Henning Urlaub,[2,3] Louis M. Staudt,[5] Kuan-Ting Pan,[4] and Eric O. Long[1,8,*]

[1]Laboratory of Immunogenetics, National Institute of Allergy and Infectious Diseases, National Institutes of Health, Rockville, MD 20852, USA
[2]Bioanalytical Mass Spectrometry Group, Max Planck Institute for Multidisciplinary Sciences, 37077 Göttingen, Germany
[3]Bioanalytics, Institute of Clinical Chemistry, University Medical Center Göttingen, 37075 Göttingen, Germany
[4]Frankfurt Cancer Institute, Goethe University, 60596 Frankfurt am Main, Germany
[5]Lymphoid Malignancies Branch, National Cancer Institute, National Institutes of Health, Bethesda, MD 20892, USA
[6]National Heart, Lung and Blood Institute, National Institutes of Health, Bethesda, MD 20892, USA
[7]Institute of Biochemistry, Kiel University, 24118 Kiel, Germany
[8]Lead contact
*Correspondence: xiaoxuan.zhuang@nih.gov (X.Z.), elong@nih.gov (E.O.L.)
https://doi.org/10.1016/j.celrep.2024.114105

SUMMARY

Natural killer (NK) cells are primary defenders against cancer precursors, but cancer cells can persist by evading immune surveillance. To investigate the genetic mechanisms underlying this evasion, we perform a genome-wide CRISPR screen using B lymphoblastoid cells. SPPL3, a peptidase that cleaves glycosyltransferases in the Golgi, emerges as a top hit facilitating evasion from NK cytotoxicity. *SPPL3*-deleted cells accumulate glycosyltransferases and complex *N*-glycans, disrupting not only binding of ligands to NK receptors but also binding of rituximab, a CD20 antibody approved for treating B cell cancers. Notably, inhibiting *N*-glycan maturation restores receptor binding and sensitivity to NK cells. A secondary CRISPR screen in *SPPL3*-deficient cells identifies B3GNT2, a transferase-mediating poly-LacNAc extension, as crucial for resistance. Mass spectrometry confirms enrichment of *N*-glycans bearing poly-LacNAc upon *SPPL3* loss. Collectively, our study shows the essential role of *SPPL3* and poly-LacNAc in cancer immune evasion, suggesting a promising target for cancer treatment.

INTRODUCTION

Natural Killer (NK) cells play a crucial role in the immune system due to their ability to recognize and kill infected or abnormal cells, including cancer cells.[1] NK cells detect target cells through a combination of activating and inhibitory receptors. Activating receptors, such as the natural cytotoxicity receptors, NKG2D, and 2B4, recognize stress-induced ligands on the surface of target cells. Inhibitory receptors, such as killer cell immunoglobulin-like receptors and NKG2A, bind to class I human leukocyte antigens (HLA-I) on healthy cells.[1–4] If the balance of activating and inhibitory signals favors activation, NK cells form tight conjugates with target cells and release the content of lytic granules to induce apoptosis in the target cell.[1] Alternatively, NK cells expressing TRAIL (*TNFSF10*) or FAS ligand (*FASLG*) engage death receptors on target cells, such as TNFRSF10 or FAS, to trigger apoptotic death. A positive correlation between the presence of NK cells and the response to immunotherapy in cancer patients has been established.[5,6] NK-focused cancer immunotherapies have shown promise for cancer treatment.[7,8] Due to a milder cytokine response and lower risk of graft-versus-host dis-

ease than T cells in allogeneic settings, NK cells are ideal candidates for use as effector cells to express chimeric antigen receptors (CARs) for immunotherapy, particularly in the development of "off-the-shelf" products.[9] Besides the killing induced by CARs, NK-cell-activating receptors engage with ligands on tumor cells and trigger additional lysis, which can provide patients with extra beneficial effects from NK-based cell therapy. The first in-human phase 1 and 2 trials using NK cells carrying a CD19-CAR to treat patients with CD19-positive non-Hodgkin lymphoma (NHL) and chronic lymphoblastic leukemia have been proven safe and have shown encouraging responses.[8]

Given the promise of NK cells as effector cells for use in treating certain cancers, it is important to determine how cancer cells could evade recognition and killing by NK cells. Although much is known about receptor-ligand interactions that regulate target cell lysis by NK cells, other pathways that may render cancer cells resistant or sensitive to NK cells have not been fully explored. These could include various intracellular changes in metabolism, lipid composition, membrane organization, and many other factors. To discover these resistance and sensitivity factors, we carried out CRISPR screens in a chronic myeloid leukemia cell line and uncovered
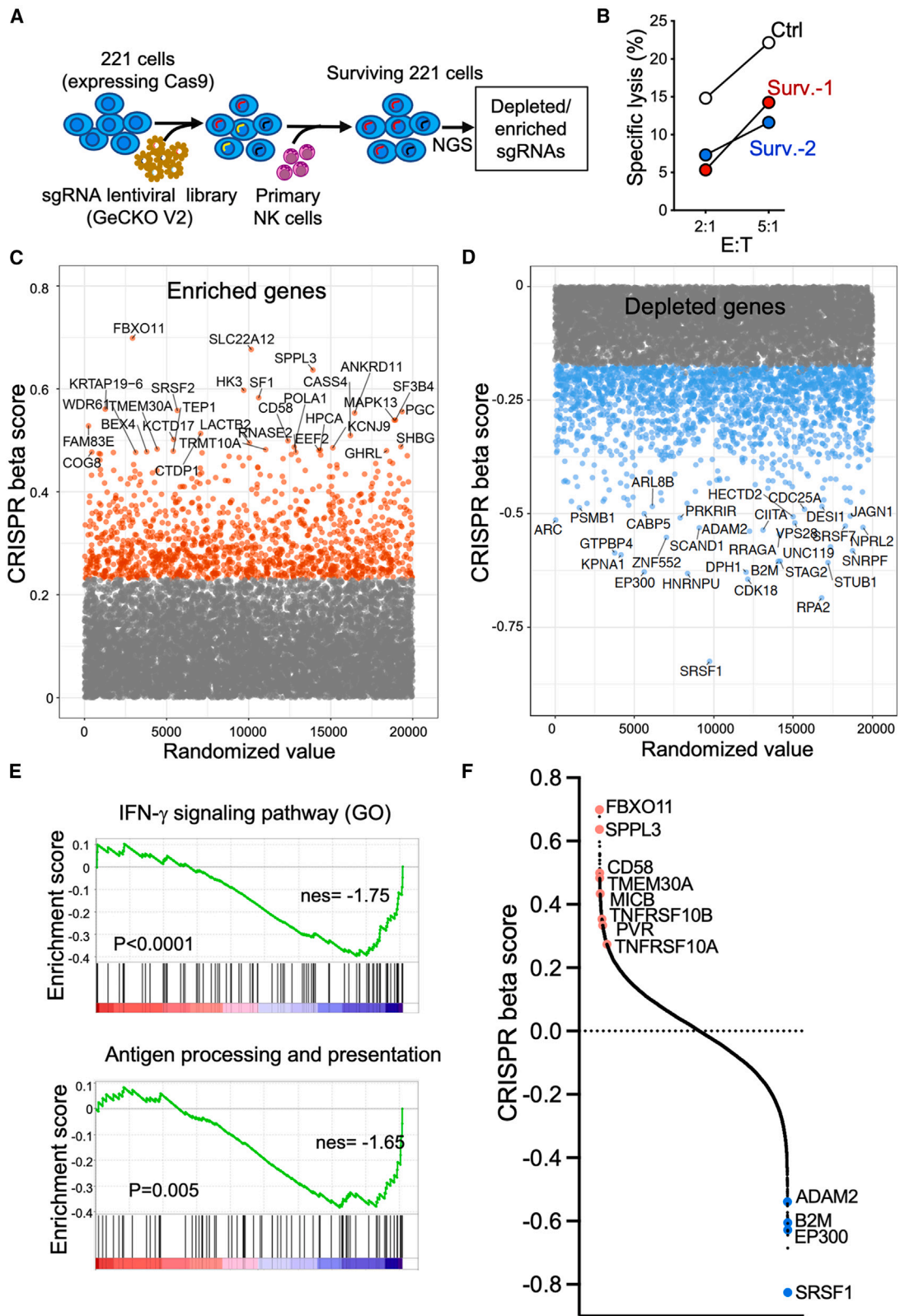
(legend on next page)

the interferon-γ (IFN-γ) signaling pathway as a strong contributor to tumor evasion,[10] as confirmed in recent studies.[11–13] By upregulating expression of HLA-I molecules on target cells, IFN-γ signaling increases the engagement of inhibitory receptors on NK cells. Conversely, the same pathway has the opposite effect on recognition and killing of tumor cells by cytotoxic CD8 T cells, due to increased presentation of tumor antigen by HLA-I.[14] The sensitivity to NK cells varies widely by tumors and cell types and is likely regulated through different pathways.

B cell malignancies, such as chronic lymphocytic leukemia and NHL, are cancers that originate from B lymphocytes. These cancers cells often evade the immune system, including their detection by NK cells, due to various mechanisms such as downregulation of cell-surface ligands that are essential for NK cell recognition and activation. For instance, mutations or deletions in *CD58*, which encodes the ligand for human receptor CD2, occur in approximately 21% of diffuse large B cell lymphomas (DLBCLs).[15] Despite these evasion mechanisms, high NK cell count remains a valid predictor of response to immunotherapy for patients with B cell malignancies.[16]

Therefore, to gain a deeper understanding of the interaction between NK cells and B cell malignancies, we performed a genome-wide CRISPR knockout screen in the 721.221 cell line (referred to hereafter as 221), an Epstein-Barr virus-transformed lymphoblastoid B cell line. This cell line had been selected for the loss of classical HLA-I genes[17] and is therefore sensitive to lysis by NK cells. As expected, the loss of ligands for NK activation receptors resulted in reduced sensitivity. Deletion of several other genes, including signal peptide peptidase-like 3 (*SPPL3*) and F-box protein 11 (*FBXO11*), had the greatest impact on promoting resistance to killing by NK cells. Here, we describe how SPPL3 functions as a crucial controller of the interaction between NK cells and their targets. We found that the increased presence of complex *N*-glycans on the surface of *SPPL3*-deleted tumor cells limits the binding of NK cell receptors and facilitates immune evasion. We further identified glycosyltransferases that were responsible for this resistance phenotype by performing a secondary CRISPR screen in *SPPL3*-deleted cells.

RESULTS

CRISPR-Cas9 screen to identify genes that regulate sensitivity to killing by NK cells

221 cells, first stably transfected with Cas9, were then stably transduced with the GeCKO V2 CRISPR library. After 10 days of puromycin selection, 221 cells were co-cultured with interleukin-2-expanded NK cells at low effector-to-target ratios of 1:10 to 1:5 until about 10%–20% of 221 cells had survived.

The surviving 221 cells were then harvested for genomic DNA extraction, library preparation, and sequencing (Figure 1A). A small proportion of these surviving cells was used in a lysis assay to confirm their reduced sensitivity to NK cells after the screen (Figure 1B). Notably, the surviving 221 cells demonstrated greater resistance to NK-mediated lysis compared to 221 cells that had been transduced with the GeCKO V2 CRISPR library but not selected by co-culture with NK cells (Figure 1B). Analysis of both enriched and depleted single guide RNAs (sgRNAs) identified novel genes that regulate sensitivity or resistance to NK-mediated killing (Figures 1C and 1D). The top 30 enriched genes included *CD58*, a known NK-activating ligand, and other new regulators such as *FBXO11* and *SPPL3* (Figure 1C). Conversely, the top 30 depleted genes included *B2M* and other resistance regulators such as *EP300* and *ADAM2* (Figure 1D). *ADAM2* has been reported to modulate the tumor necrosis factor (TNF) response in tumor cells,[18] whereas the function of *EP300* in this context is unknown. Gene set enrichment analysis revealed that sgRNAs targeting genes in the IFN-γ and antigen-presentation pathways were depleted (Figure 1E). The screen enriched gRNAs targeting other ligands for NK cell receptors such as *MICB*, *PVR*, *TNFRSF10B*, and *TNFRSF10A* (Figure 1F), which engage NK receptors NKG2D (*KLRK1*), DNAM-1 (*CD226*), and TRAIL (*TNFSF10*), respectively. *TMEM30A*, an essential component of the phospholipid phosphatidylserine (PS) flippase, was also among the top enrichment hits. Loss of this gene led to exposure of PS on the tumor cell surface and resistance to T cells and NK cells through sensing of exposed PS by the inhibitory receptor Tim-3 (*HAVCR2*) (Figure 1F).[19]

To validate the top hits, we performed killing assays on 221 cells edited with a non-targeting sgRNA (sgNT) or sgRNA targeting a single gene of interest. These cells were pre-labeled with different combinations of fluorescent membrane dyes (Figures 2A and 2B), mixed with NK cells at a 1:1 ratio and incubated for 16 h with NK cells (Figure 2A). Flow cytometry was used to determine changes in cell ratios after co-culture. Knockouts of NK receptor ligands *MICB*, *CD58*, *TNFRSF10B*, and *TNFRSF10A* were more resistant to NK-cell-mediated killing compared to sgNT 221 cells (Figure 2B). The knockout efficiency of sgRNAs targeting these genes was validated by staining with antibodies (Figure S1A). Deletions of regulators *FBXO11* and *SPPL3* resulted in greatly reduced sensitivity to killing (Figure 2B), and the sgRNAs targeting these genes efficiently reduced their expression (Figures S1B and S1C). The guide sgSPPL3-1, exhibiting superior knockout efficiency compared to sgSPPL3-2, was chosen for further experiments unless otherwise specified (Figure S1B). 221 cells expressing sgRNA for *MICB*, a ligand of receptor NKG2D, stimulated less degranulation by NK cells (Figure 2C). Deletion of *CD58*, the ligand

Figure 1. CRISPR-Cas9 screen to identify genes that regulate sensitivity to NK cells
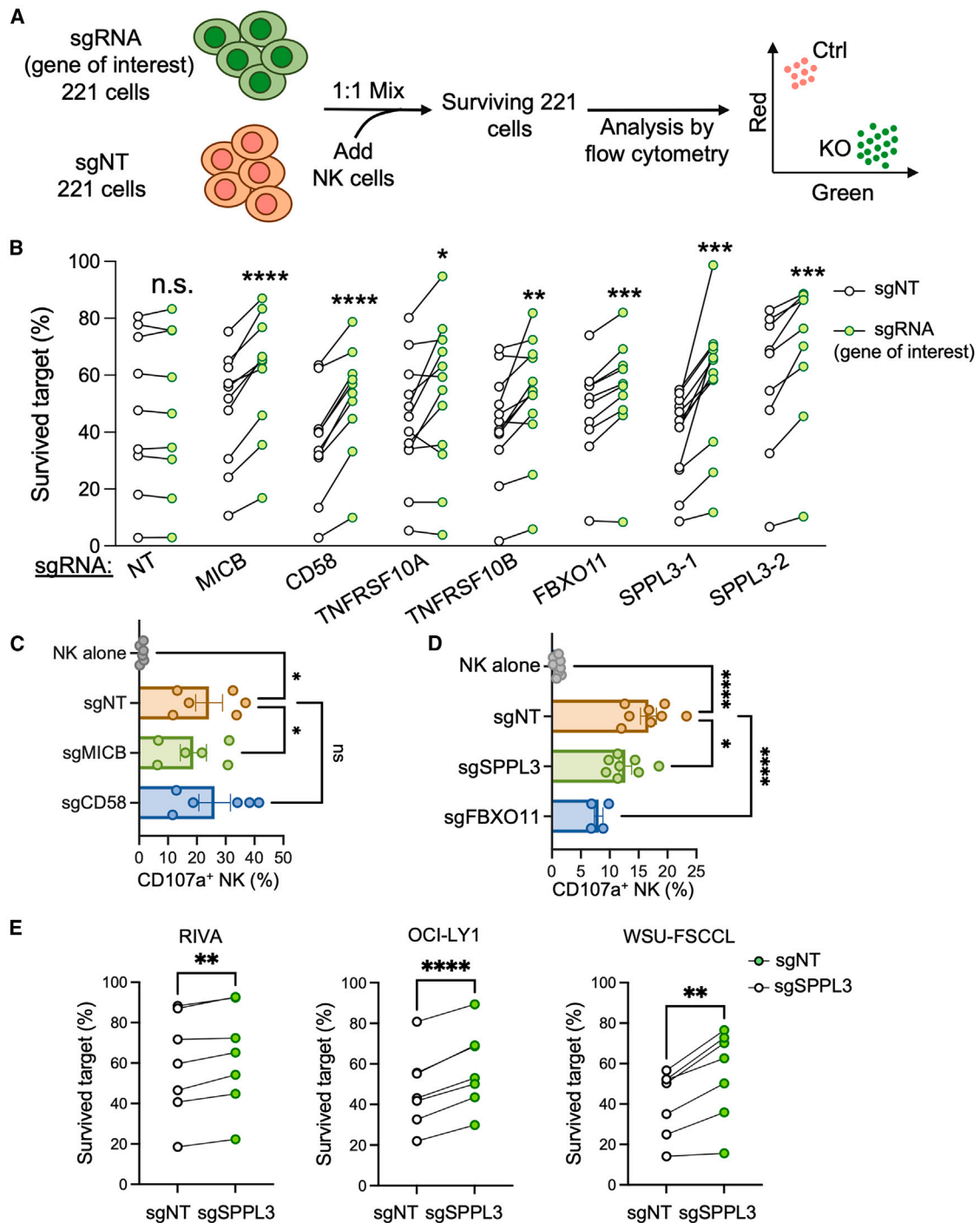(A) Experimental outline of the genome-wide CRISPR knockout screen in 221 cells. 221-Cas9 cells transduced with the sgRNA library were co-incubated with activated primary human NK cells. Distribution of sgRNAs in the surviving 221 cells was analyzed by NGS.
(B) Representative killing assay to test resistance after the screen by flow cytometry with 221 cells that survived co-culture with NK cells (Surv.-1 and Surv.-2) or 221 cells cultured without NK cells (Ctrl).
(C and D) Scatterplots showing enriched (C) and depleted (D) genes in the screen. CRISPR scores were calculated via the MAGeCK MLE analysis (y axis). Each dot represents a gene, and the top 30 enriched (C) and depleted (D) genes are labeled.
(E) Gene set enrichment analysis of CRISPR scores of depleted genes and their relationship with IFN-γ signaling and antigen processing and presentation pathways.
(F) Ranked plot of CRISPR scores from the screen in 221 cells. Highlighted genes are color-coded red for enriched genes and blue for depleted genes.

Figure 2. Validation of CRISPR screen hits

(A) Experimental outline of the killing assay used to validate hits from the CRISPR screen. 221 cells expressing non-targeting sgRNA (sgNT) and sgRNA targeting genes of interest were pre-labeled with dyes and mixed at a 1:1 ratio before co-culture with NK cells. Surviving 221 cells were analyzed by flow cytometry.

(B) Killing assays using activated NK cells and 221 target cells expressing sgRNAs for the indicated genes (green circles) compared to cells expressing sgNT (white circles). *SPPL3* was deleted separately with two different sgRNAs. Each line represents an independent donor ($n \geq 8$, paired t test; n.s., not significant; $*p < 0.05$, $**p < 0.01$, $***p < 0.001$, $****p < 0.0001$).

(C) NK cell degranulation induced by 221 cells expressing sgNT or sgRNAs targeting genes encoding the NK cell ligands MICB and CD58. Data shown as mean ± SEM ($n = 6$; $*p < 0.05$; ns, not significant).

(legend continued on next page)

for CD2, had a greater impact on killing but did not change NK degranulation by NK cells (Figure 2C). This is consistent with the function of CD2 in adhesion and other activation receptors on degranulation.[20,21] Knockouts of *SPPL3* and *FBXO11* also resulted in a reduced stimulation of NK cell degranulation (Figure 2D). *FBXO11* encodes one of the components of an E3 ubiquitin ligase complex that promotes the degradation of transcriptional regulators, such as BCL6[22] and CIITA.[23] In the absence of *FBXO11*, BCL6 and CIITA are stabilized. BCL-6 promotes B cell differentiation and facilitates apoptosis of germinal center B cells via suppression of *BCL2*, an anti-apoptotic gene,[22,24] and CIITA upregulates major histocompatibility complex class II gene transcription.[25] As *SPPL3* deletion was strongly associated with protection of the acute lymphoblastic leukemia (ALL) B cell ALL (B-ALL) line NALM6 from lysis by CD19-CAR-T cells[26] (Figure S1D) and by NK cells[27] (Figure S1E), we focused our effort on SPPL3.

SPPL3 acts as a central regulator of active Golgi glycotransferases and cellular glycosylation,[28] prompting our interest in exploring the role of glycosylation in the regulation of NK-tumor interactions. We performed *SPPL3* knockout in several patient-derived DLBCL cell lines (RIVA, OCI-LY1, and WSU-FSCCL) and observed a consistent increase in resistance to NK-mediated killing upon *SPPL3* deletion in these cell lines (Figures 2E and S1F). These results suggest a shared NK evasion mechanism arising from *SPPL3* deletion and the modification of cellular glycosylation status in malignant B cells.

Increased glycosylation of ligands for NK receptors and reduced binding of soluble receptors to *SPPL3*-deleted cells

To further investigate the effect of *SPPL3* deletion, we examined the expression of several ligands of NK receptors on *SPPL3*-deleted 221 cells (Figures S2A–S2E). Surface levels of CD48, CD58, ICAM-1, CD80, HLA-E, and MICB were unchanged in *SPPL3*-deficient cells (Figures S2A and S2B). RNA-sequencing (RNA-seq) analysis was performed to examine the expression of various ligands of NK receptors in sgNT and sgSPPL3 221 cells. The cells were clustered into respective groups in a principal component analysis (Figure S2C). The transcriptional levels of ligands such as *TNFRSF1A/B*, *TNFRSF10 A/B*, *SLAMF7/6*, *PVR*, *MICB*, *ICAM*1, *HLA-E*, *FAS*, *CD80*, *CD70*, *CD58*, *CD48*, and *CD27* were not affected (Figure S2D). SPPL3 deletion resulted in minor changes in the transcriptome of 221 cells, with a significant upregulation of only two genes and downregulation of six genes (Figure S2E). Most of these genes are expressed at a low level (log counts per million [CPM] < 4), and none of them encode ligands for NK cell receptors. The two differentially expressed genes (IGL and RNR1) with higher expression levels (logCPM > 4) are not relevant to NK-tumor interaction.

SPPL3 is a Golgi-resident intramembrane protease that cleaves the catalytic domain of glycosyltransferases from their membrane anchors, which could promote their secretion into the extracellular space and lead to a reduced intracellular abundance and, thus, activity of these enzymes.[28,29] MGAT5 is one of the best-studied glycosyltransferases that are cleaved and regulated by SPPL3.[29] We monitored MGAT5 protein levels in cell lysates and supernatants of 221 cell cultures (Figure 3A). *SPPL3*-deficient 221 cells had increased cellular expression of MGAT5 and a decreased amount of MGAT5 released into the culture media, suggesting that MGAT5 is retained inside *SPPL3*-deficient cells where it promotes increased glycosylation and branching of *N*-glycans (Figure 3A). To test this, we stained 221 cells with the lectin concanavalin A (ConA) to detect high mannose and *Sambucus nigra* lectin (SNA) to determine the extent of sialylation. *SPPL3*-knockout cells had reduced high mannose and increased terminal sialic acid glycans (Figure 3B), indicating a shift toward more complex glycans. To examine the glycosylation status of several ligands for NK receptors, we performed motility-shift experiments and found that glycosylation of CD58 was greatly increased in *SPPL3*-knockout 221 cells (Figure 3C). Similarly, hemagglutinin (HA)-tagged versions of MICB and PVR transfected into 221 cells showed reduced mobility in *SPPL3*-knockout cells (Figure 3D). To test whether increased glycosylation of ligands could interfere with receptor interaction, we measured binding of soluble recombinant receptors NKG2D and CD2 to sgSPPL3 221 cells. Binding of either receptor to *SPPL3*-deficient cells was decreased as compared to binding with control sgNT 221 cells (Figures 3E and 3F), presumably due to steric hindrance by larger *N*-glycans on MICB and CD58. Similar reduced binding of recombinant CD2 was also observed on *SPPL3*-deleted RIVA, OCI-LY1, and WSU-FSCCL DLBCL cells (Figure S3). The reduced binding of soluble CD2 to *SPPL3*-deleted cells was only partial, which could be due to greater accessibility of soluble CD2 to CD58, as compared to transmembrane CD2, which is restricted through interactions in *cis* with other molecules at the plasma membrane, such as CD16.[30] Heavily glycosylated CD58 on target cells may also interfere with the ability of CD2 to engage in other functional interactions.

If our interpretation was correct, the effect of *SPPL3* deletion and enhanced *N*-glycosylation should be reversed by inhibition of the *N*-glycan pathway. Therefore, we treated both sgNT and sgSPPL3 221 cells with kifunensine, a potent inhibitor of mannosidase I (Figure 4A). Trimming of high-mannose forms by mannosidase I is essential for the synthesis of complex *N*-glycan forms. Using the lectin ConA specific for terminal mannose residues, which are exposed prior to trimming, we observed much higher staining of kifunensine-treated sgNT and sgSPPL3 cells as compared to untreated cells (Figures 4A and 4B). After treatment with kifunensine, the difference in ConA staining between untreated sgNT cells and sgSPPL3 cells was eliminated (Figure 4B). Kifunensine also prevented the maturation of large glycans on CD58 and MICB, as determined by electrophoretic motility (Figures 4C and 4D). Notably, kifunensine treatment restored NK cell degranulation stimulated by SPPL3-deficient 221 cells (Figure 4E) and reinstated the binding of soluble recombinant CD2 to these cells (Figure 4F).

(D) NK cell degranulation induced by 221 cells expressing sgNT or sgRNAs targeting SPPL3 and FBXO11. Data shown as mean ± SEM ($n = 8$, one-way ANOVA; *$p < 0.05$, ****$p < 0.0001$).

(E) Killing assays using activated NK cells and the indicated DLBCL cell lines expressing sgSPPL3 (green circles) compared to cells expressing sgNT (white circles) ($n = 8$, paired t test; *$p < 0.05$, **$p < 0.01$, ****$p < 0.0001$).
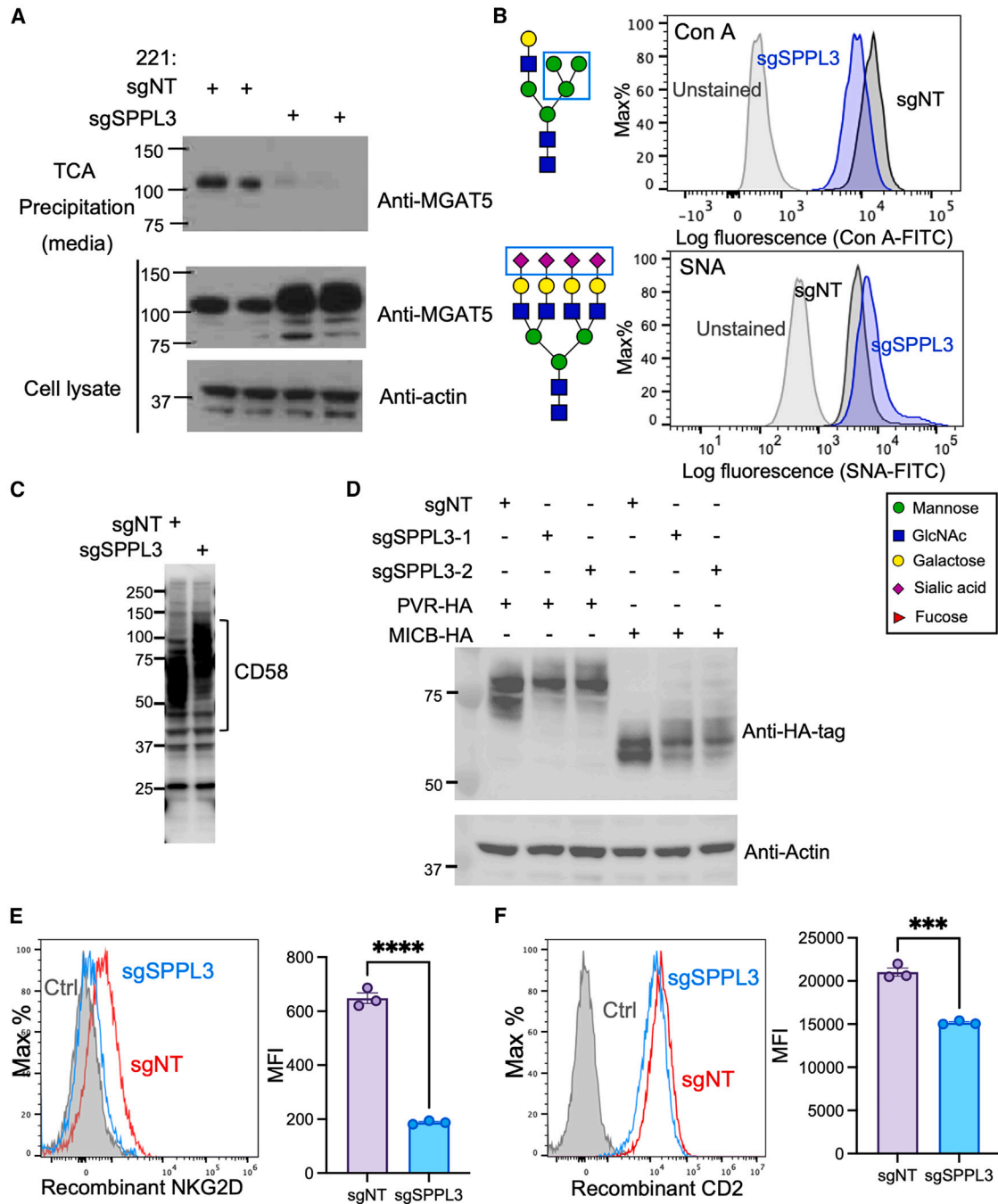
Figure 3. Impact of SPPL3 deletion on glycosylation of ligands for NK receptors and on binding to their receptors

(A) Immunoblot of MGAT5 in TCA-precipitated culture supernatants (top) and in total cell lysates (center) of sgNT-expressing and SPPL3 knockout cells. Immunoblot of actin was used as loading control (bottom).

(B) Representative histograms of lectins ConA and SNA binding to 221 cells expressing sgNT or sgSPPL3 (blue). The binding specificities for glycan structures (blue box) are shown using the standard symbols for glycans (shown in box).

(C) Immunoblot of CD58 in total cell lysates of SPPL3-knockout 221 cells versus sgNT 221 cells.

(D) Immunoblot of HA-tagged PVR and MICB transfected into SPPL3-deleted 221 cells and sgNT 221 cells. Whole-cell lysate was immunoblotted with antibodies to HA and actin.

(E and F) Representative histograms and statistical bar graphs show binding of soluble recombinant NK cell receptors NKG2D and CD2 to 221 cells transfected with sgNT (red) or sgSPPL3 (blue). Ctrl represents staining using a recombinant human IgG1 Fc (gray). $n = 3$, unpaired t test; ****$p < 0.0001$, ***$p < 0.001$.
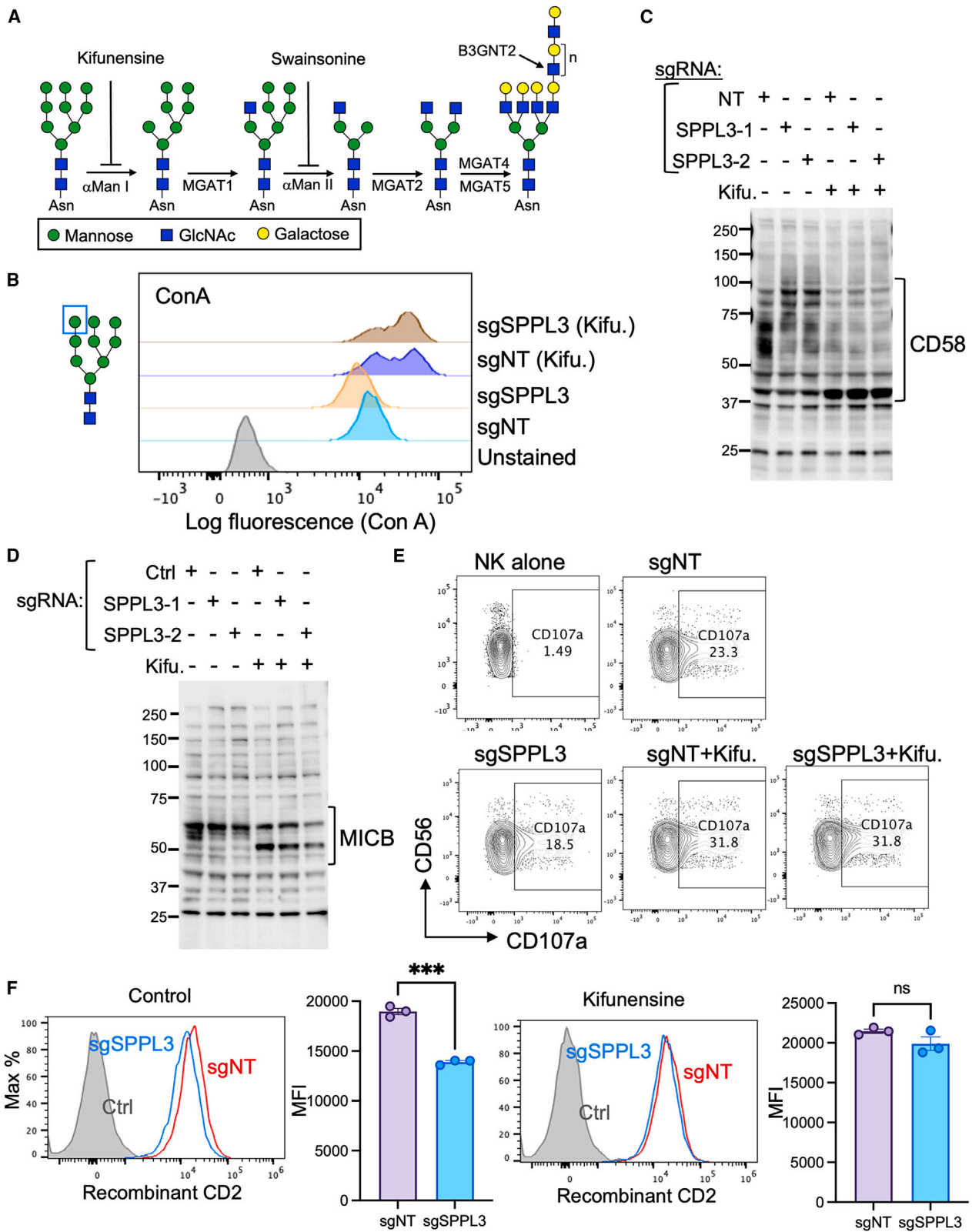
(legend on next page)

Disruption of the *N*-glycan maturation pathway increased the sensitivity of *SPPL3*-deleted 221 cells to NK-mediated killing

Next, the sensitivity of kifunensine-treated 221 cells to NK-mediated killing was evaluated. sgNT and sgSPPL3 221 cells treated or not with kifunensine were barcoded using different concentrations of PKH26 (red) and PKH67 (green) dyes and mixed at a 1:1:1:1 ratio (Figure 5A). Their relative sensitivity to NK-mediated killing was then assessed using flow cytometry (Figure 5A). *SPPL3*-deleted cells were more resistant to killing than sgNT cells, and kifunensine treatment reverted the sensitivity of SPPL3-deleted cells back to the level of killing observed with sgNT-treated 221 cells (Figure 5B). To confirm the specificity of kifunensine, we repeated the killing assay using another glycosylation inhibitor, swainsonine, which blocks a later step in glycan maturation executed by the Golgi-resident α-mannosidase II (Figure 4A). Similarly, the greater resistance of sgSPPL3 221 cells to NK-mediated killing disappeared after swainsonine treatment (Figure 5C). Both kifunensine and swainsonine reduced the amount of complex glycans at the cell surface that were detected by the lectin PHA-E (*Phaseolus vulgaris* erythroagglutinin) on sgNT and sgSPPL3 221 cells (Figure S4).

In addition to impairment of receptor-ligand interactions at the NK-target cell synapse, heavy glycosylation may also impair the binding of antibodies to tumor cell antigens and prevent the ability of NK cells to perform antibody-dependent cellular cytotoxicity (ADCC). This is relevant in the context of monoclonal antibody therapies that target tumor antigens. The CD20 antibody rituximab is one of the most established antibodies used to treat various B cell malignancies.[31] Binding of rituximab to 221 cells deficient in SPPL3 was indeed reduced (Figures 5D and 5E). Cells lacking SPPL3 were more resilient to CD20-dependent NK-cell-mediated ADCC, and their resistance to ADCC was restored by treatment with kifunensine (Figure 5F).

A secondary CRISPR screen in *SPPL3*-knockout cells to identify SPPL3 substrates that are responsible for resistance to NK-cell-mediated lysis

To gain insight into how glycan structures of ligands on 221 cells for NK receptors can impact the sensitivity of 221 cells to NK-dependent killing, a CRISPR screen focused on glycosylation pathways[32] was performed with *SPPL3*-knockout cells (Figure 6A). Cumulative CRISPR scores (CSSs) were determined by subtracting the CSS of sgNT cells from the CSS of sgSPPL3 cells, as displayed in Figure 6B. *B3GNT2* was one of the top depleted hits that restored sensitivity of *SPPL3*-knockout cells to NK-cell-dependent killing (Figures 6A and 6B). *B3GNT2* encodes the main glycosyltransferase that extends highly branched *N*-glycans by transfer of an *N*-acetylglucosamine

(GlcNAc) moiety in a β1,3 linkage with a terminal unsialylated galactose, preferentially on the MGAT5-generated β-1,6-linked branch in tri- and tetra-antennary *N*-glycans.[33] The subsequent transfer of Gal in a β1,4 linkage to GlcNAc by a B4GALT transferase generates the disaccharide *N*-acetyl-lactosamine (LacNAc). Iterations of B3GNT2- and B4GALT-mediated transfers generate additional poly-LacNAc extensions (Figure 4A). We used the lectin LEL (*Lycopersicon esculentum* lectin), which binds preferentially to LacNAc, to test for the presence of LacNAc on 221 cells. The stronger binding of LEL to the plasma membrane of sgSPPL3 cells, as compared to sgNT 221 cells, indicated an increased amount of LacNAc (Figure 6C). Deletion of *B3GNT2* in both sgNT and sgSPPL3 cells drastically reduced LEL binding to these cells (Figure 6D). In addition, the loss of B3GNT2 in 221 cells restored the ability of NK cells to degranulate in response to stimulation by *SPPL3*-knockout cells (Figure 6E). These findings suggest that the reduced activation of NK cells by *SPPL3*-deleted 221 cells is due to the presence of complex *N*-glycan structures, including tri- and tetra-antennary branching and their extension with additional LacNAc.

Furthermore, the screen showed that deletion of other genes involved in *N*-glycosylation, such as *MGAT2* and *MGAT4B*, resulted in increased sensitivity of *SPPL3*-knockout cells (Figure 6B), indicating that branching into complex *N*-glycans by MGATs contributed to resistance. Deletion of *MGAT3* had the opposite effect (Figure 6A), consistent with the inhibition of MGAT4- and MGAT5-mediated branching imposed by MGAT3-dependent *N*-glycan bisection.[34,35]

Glycoproteomic and glycomic analysis of *N*-glycans on cells lacking *SPPL3*

Analysis of the glycoproteome of sgSPPL3 and sgNT 221 cells revealed 273 unique glycans and 5,132 intact glycopeptides. Figure 7A displays the structure of identified *N*-glycans that carried four branches and elongation of at least one branch. Cells lacking SPPL3 displayed a higher presence of such complex *N*-glycans (having at least eight Hex and seven HexNAc) as compared to the control cells (Figure 7B). This trend was validated through the analysis of unique intact glycopeptides, whereby we observed an increase in glycopeptides with complex glycan structures under the SPPL3-knockout condition (Figure 7C). Direct comparison of glycan abundance in sgPPL3 cells and sgNT cells confirmed that tetra-antennary *N*-glycans with elongation (at least eight Hex and seven HexNAc) is upregulated in SPPL3-deleted cells (Figure 7D), whereas the change of A3B/A4 glycans was not significant (Figure 7E). The glycoproteome analysis identified high-molecular-mass glycans on abundant proteins only. ICAM-1, the ligand binding to integrin LFA-1 on NK cells, and CD48, which binds to the NK-cell-activating

Figure 4. Inhibition of *N*-glycan maturation reduced the glycosylation of ligands for NK receptors and restored NK cell degranulation induced by SPPL3-knockout 221 cells

(A) Diagram of *N*-glycan maturation from the high-mannose stage. The mannosidase I inhibitor kifunensine and the mannosidase II inhibitor swainsonine inhibit the trimming of high-mannose glycans.

(B) ConA staining of sgNT and sgSPPL3 221 cells, treated or not with kifunensine, as indicated.

(C and D) Immunoblots of CD58 (C) and MICB (D) in sgNT and SPPL3-knockout 221 cells, treated or not with kifunensine.

(E) Representative contour plots of surface CD107a expression on NK cells stimulated with sgNT and sgSPPL3 221 cells.

(F) Representative histograms and statistical bar graphs of recombinant CD2 binding to sgNT and sgSPPL3 cells before and after kifunensine treatment. Ctrl represents staining using a recombinant human IgG1 Fc (gray). *n* = 3, unpaired t test; ***$p < 0.001$; ns, not significant.
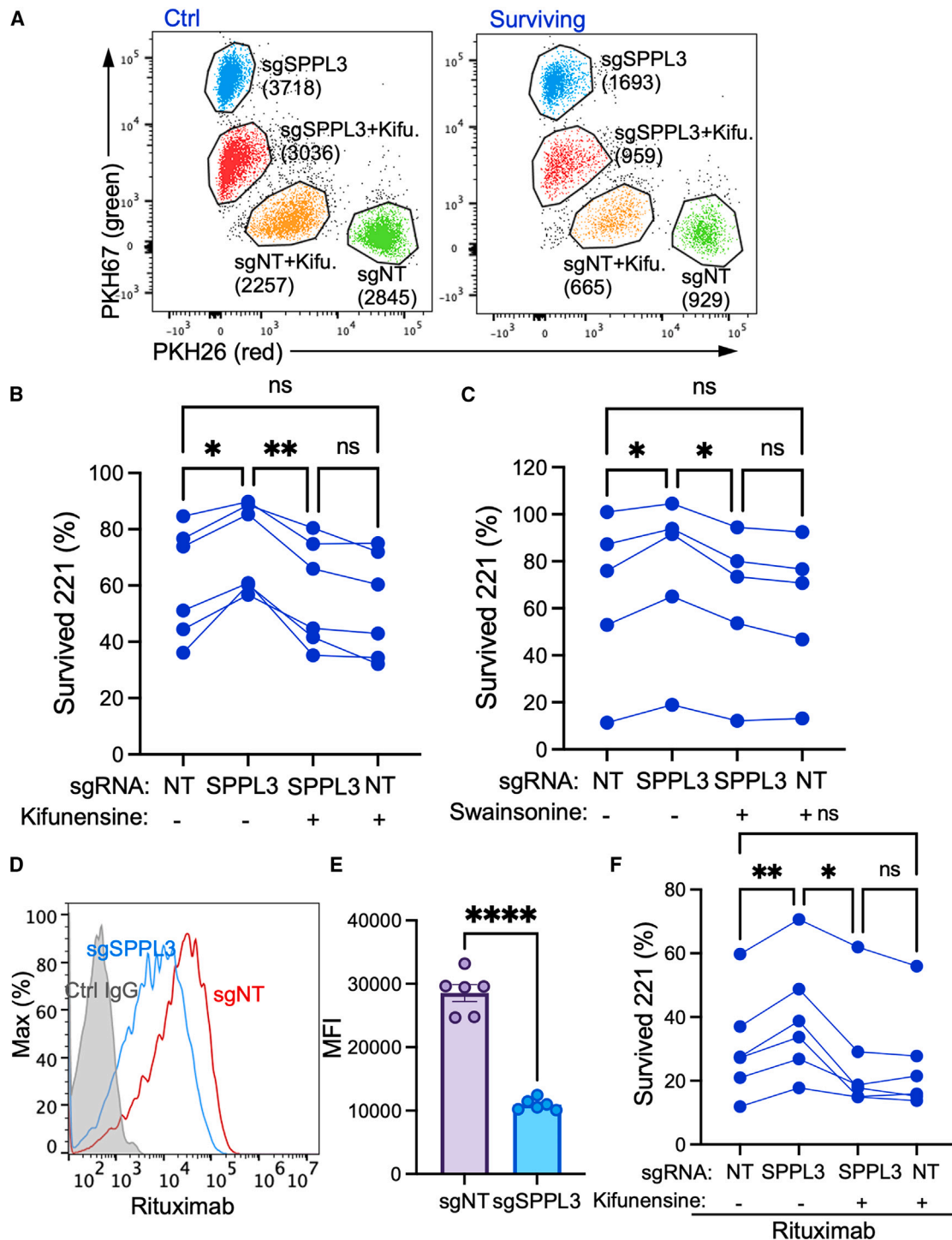
Figure 5. Treatment with *N*-glycosylation inhibitors restored the sensitivity of SPPL3-deleted 221 cells to NK-mediated killing and ADCC

(A) Representative dot plots of flow-cytometry analysis of color-coded sgNT or sgSPPL3 221 target cells in a killing assay with NK cells. Cells were treated or not with kifunensine.

(B) Statistics using NK cells from independent donors as in (A). Each line represents a different donor ($n = 6$, paired one-way ANOVA; ns, not significant; *$p < 0.05$, **$p < 0.001$).

(C) Statistics of color-coded killing assays to compare sensitivity of sgNT- and sgSPPL3-expressing 221 cells, which were either non-treated or treated with the Golgi α-mannosidase II inhibitor swainsonine. Each line represents an independent donor ($n = 6$, paired one-way ANOVA; ns, not significant; *$p < 0.05$).

(D) Histograms of rituximab staining of 221 cells expressing sgNT (red) or sgSPPL3 (blue).

(legend continued on next page)

receptor 2B4 (*CD244*), each carried at least one tetra-antennary glycan that was elongated with terminal LacNAc moieties (Table S1). To obtain more information on the composition of *N*-glycans in *SPPL3*-knockout cells, we performed a glycomic analysis by releasing glycans and acquiring mass spectrometry data on these glycans only. Glycomic analysis can focus on larger *N*-glycan species that are difficult to characterize in glycoproteome analysis (Figure S5). The *SPPL3* knockout resulted in an increase of complex *N*-glycans, including higher-mass glycans carrying longer poly-LacNAc extensions (Figure S5).

DISCUSSION

The goal of this study was to identify genes that promote resistance of target cells against NK cell attack. Such information could unveil immune evasion mechanisms employed by tumors, offering possible targets for cancer therapy. One of the genes with the strongest evasion scores in a genome-wide CRISPR screen for resistance to NK cells was *SPPL3*. SPPL3 is an intramembrane protease located in the Golgi apparatus that cleaves glycosyltransferases in their transmembrane region and releases their catalytic domain.[28,29,36] The activity of SPPL3 reduces the accumulation of intracellular glycosyltransferases and moderates the protein glycosylation level as they transit through the Golgi. Accordingly, *SPPL3* deletion in the B cell lymphoblastoma cell line 221 led to an increase in complex *N*-glycans on plasma membrane proteins. Biochemical and functional experiments revealed that increased glycosylation of ligands for NK activation receptors NKG2D and CD2 interfered with receptor binding and lysis of the target cells by NK cells. This effect was validated across various patient-derived DLBCL cell lines, pointing to a shared NK evasion mechanism driven by the deletion of SPPL3 in malignant B cells. Analysis of ligands for NK receptors in *SPPL3*-knockout 221 cells revealed slower migration during gel electrophoresis, consistent with higher glycosylation. Pharmacological inhibition of the *N*-glycan pathway—at a step preceding branching mediated by MGAT transferases—reversed the slower gel migration of ligands and restored normal sensitivity of *SPPL3*-KO 221 cells to lysis by NK cells.

Notably, SPPL3 ranks among the very top genes deleted in The Cancer Genome Atlas lung adenocarcinoma patients.[37] In addition, previous research has linked the loss of a chromatin regions encompassing *SPPL3* to reduced infiltration of T cells in lung adenocarcinoma.[38] This may be due to elevated glycosylation and disruptions in ligand-receptor interactions. Our study suggests that NK cells may also be impaired in this respect. Unlike mutations in specific ligands for NK receptors, the impact of *SPPL3* mutations in cancer is much broader. Therefore, we investigated the molecular basis for this association of *SPPL3* deletion and cancer immune evasion. Using an sgRNA library focused on glycosylation for a secondary CRISPR screen in *SPPL3*-knockout cells, we showed that enzymes promoting high branching of *N*-glycans and their elongation by addition of

LacNAc were the main contributors to the evasion of *SPPL3*-deleted cells from lysis by NK cells.

NK cells lyse target cells mainly through two distinct pathways. One is the delivery of lytic effector molecules, such as granzymes, into target cells through membrane pores formed by polymerization of perforin. The second is through engagement of death receptor on target cells by TRAIL (*TNFSF10*), which is highly expressed on NK cells. Deletion of two death receptor genes *TNFRSF10A* and *TNFRSF10B* contributed to resistance in the primary genome-wide screen, suggesting that TRAIL on NK cells, which binds to both receptors, contributed to 221 cell death during selection in co-culture. Over time, NK cells switch from rapid granzyme B-mediated killing to slower death-receptor-induced killing.[39] Given the long-term incubation and low effector-to-target ratio with primary NK cells used in the selection for resistant mutants, both pathways were given a chance to participate in elimination of target cells. A contribution of apoptosis to cell death of 221 cells in our screen was supported by deletions of *SRSF1* and *SRSF2* genes, which encode splicing factors of the Ser/Arg family (SRSF). SRSF1 promotes RNA splicing that prevents apoptosis, whereas SRSF2 promotes apoptosis.[40,41] In the genome-wide screen, *SRSF1* was among depleted sgRNAs and *SRSF2* was among enriched sgRNAs, consistent with the anti- and pro-apoptosis function of SRSF1 and SRSF2, respectively.

Deletion of genes encoding ligands (CD58, MICB, PVR) of NK activation receptors also resulted in reduced sensitivity to NK cells. Their evasion score was lower because activation of NK cells requires co-engagement of several activation receptors.[20] The enhanced glycosylation of CD58 and MICB in *SPPL3*-knockout cells interfered directly with binding of soluble receptors CD2 and NKG2D, respectively. Steric hindrance was likely responsible for this disruption, considering that two distinct and specific ligand-receptor interactions were inhibited. Furthermore, receptor binding and activation of NK cell cytotoxicity were recovered after pharmacological inhibition of the *N*-glycosylation pathway at an early step, prior to the branching mediated by MGAT transferases. In addition, binding of the CD20 antibody rituximab was impaired on *SPPL3*-knockout cells. This suggests that escape from treatment of mature B cell NHL and mature B-ALL with rituximab can occur not only by downregulation of CD20 (*MS4A1*) expression but also by enhanced CD20 glycosylation. This should be an important consideration in the selection of antibodies for both monoclonal antibody therapies and single-chain variable fragments (scFvs) inserted into CARs.

Pathways previously known to protect or sensitize target cells facing an attack by NK cells were identified, providing a strong validation of our genetic screens. *B2M* knockout on its own increased sensitivity to NK cells, and pathway analysis showed that several other genes involved in antigen processing and presentation pathways significantly scored in mediating resistance to NK cells. 221 cells lack expression of classical HLA class I molecules but do express HLA-E, a ligand for inhibitory receptor

---

(E) Statistics of several experiments performed as in (D). Data are shown as mean ± SEM ($n = 6$, unpaired t test; ****$p < 0.0001$).

(F) Statistics from killing assays to compare the sensitivity of 221 cells expressing sgNT or sgSPPL3 to NK-mediated ADCC triggered by 10 μg/mL rituximab. Cells were treated or not with kifunensine, as indicated. Each line represents NK cells from different donors ($n = 6$, paired one-way ANOVA; ns, not significant; *$p < 0.05$, **$p < 0.01$).
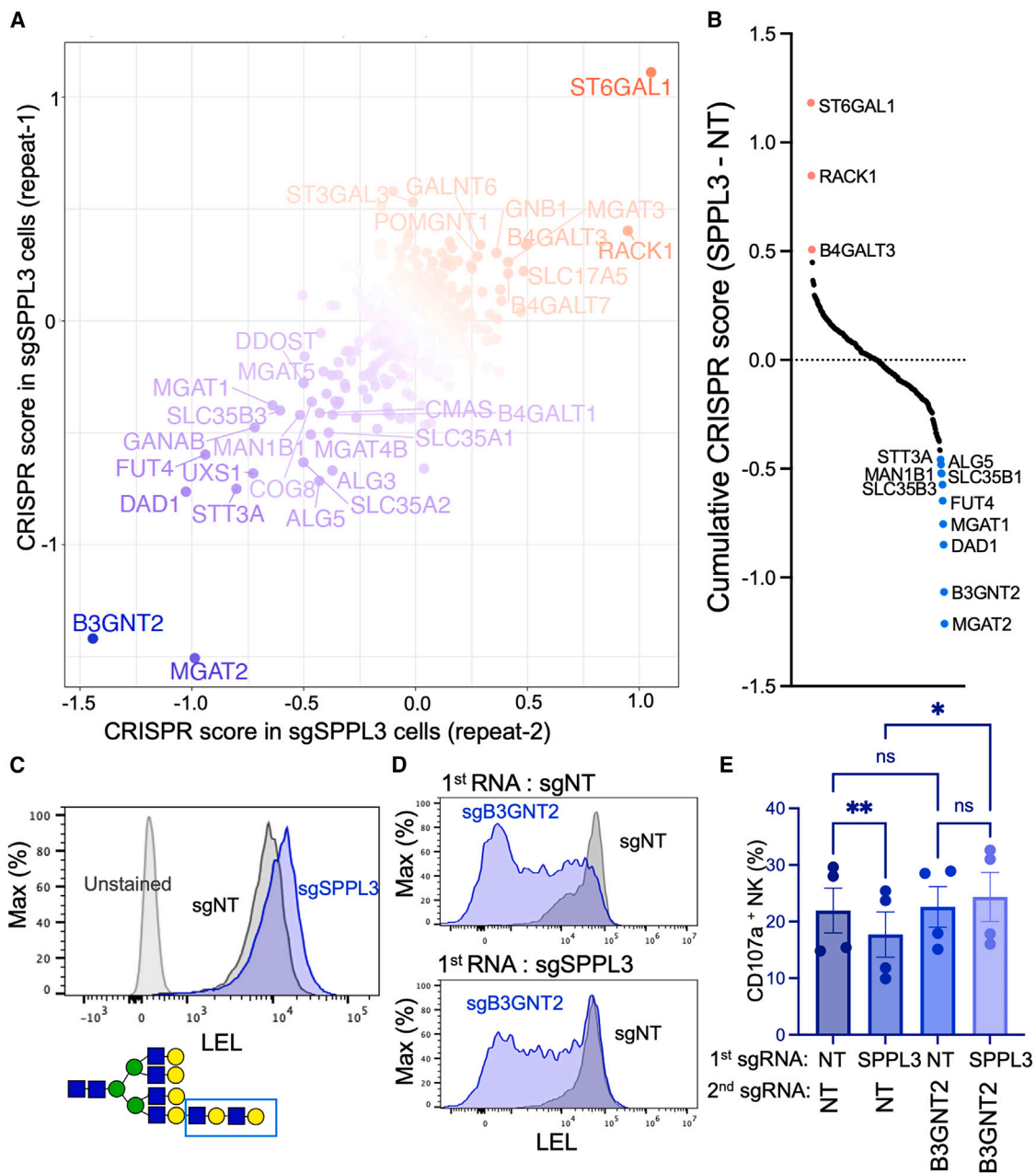
Figure 6. Secondary CRISPR screen in SPPL3-deficient 221 cells to identify glycosyl transferases responsible for the inhibition of NK-mediated killing

(A) CRISPR knockout screen in *SPPL3*-deleted 221 cells using a glycosylation-focused sgRNA sublibrary. 221 cells expressing the library were co-cultured with activated primary NK cells. Distribution of sgRNAs in surviving 221 cells was analyzed by NGS. Two biological repeats were plotted on the x axis and y axis, respectively. CRISPR beta scores were calculated using the MAGeCK MLE method. Enriched genes, signifying greater resistance, are shown in red, whereas depleted genes, signifying greater sensitivity, are in blue. Gene names of top hits are shown.

(B) Ranked plot of cumulative CRISPR scores calculated by the score from SPPL3-knockout cells minus the score from 221 cells expressing sgNT.

(C) Representative histograms of LEL binding to sgNT (top) or sgSPPL3 (bottom) 221 cells.

(D) Representative histograms of LEL binding to SPPL3-knockout 221 cells expressing two individual sgRNAs with the first sgRNA being sgNT (top) or sgSPPL3 (bottom) and the second sgRNA either non-targeting or against *B3GNT2*.

(E) NK cell degranulation stimulated by 221 cells expressing two individual sgRNAs as in (D). Each dot represents NK cells from an independent donor ($n = 4$, paired one-way ANOVA; ns not significant; *$p < 0.05$, **$p < 0.01$).
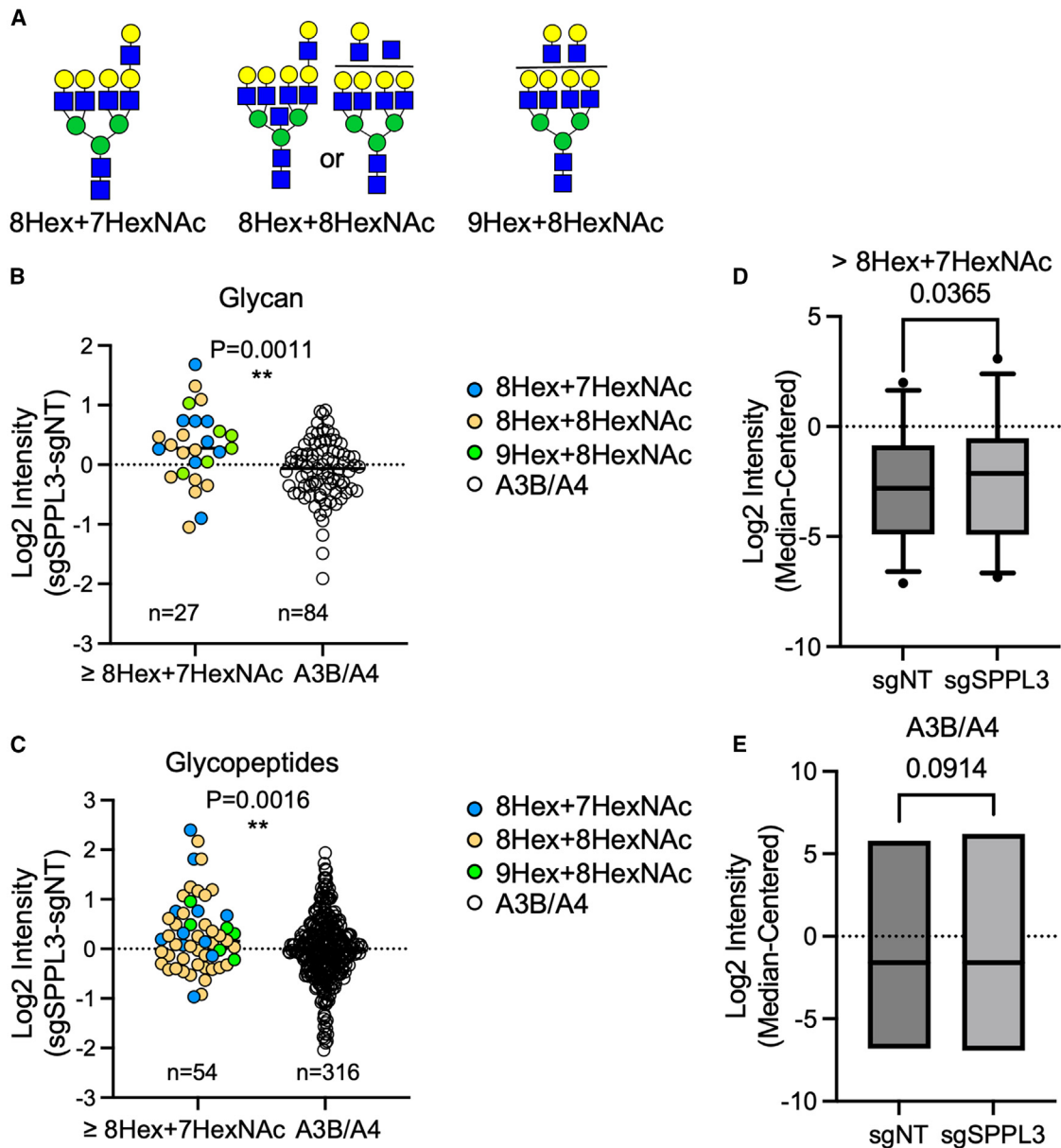
Figure 7. High-molecular-mass *N*-glycans on SPPL3-deficient cells

(A) Diagram of *N*-glycans carrying at least eight hexoses (Man and Gal) and seven HexNacs (GlcNAc) that were identified by glycoproteomic analysis of sgNT and sgSPPL3 221 cells.

(B) Relative abundance of glycans shown in (A) compared to all other tri- and tetra-antennary (A3B/A4) glycans. Log_2 intensity values from SPPL3-deleted cells minus values from sgNT cells are shown on the y axis (unpaired t test, **$p < 0.01$).

(C) Same comparison as in (B) but for intact glycopeptides (unpaired t test, **$p < 0.01$).

(D) Box plot comparing median-centered log_2 intensity of glycans as shown in (A) (unpaired t test).

(E) Box plot comparing median-centered log_2 intensity of other tri- and tetra-antennary (A3B/A4) glycans (unpaired t test).

See also Table S1.

NKG2A. Likewise, the IFN-γ signaling pathway, which upregulates HLA class I expression and antigen processing, was a significant protector against lysis by NK cells, as reported previously.[10,42] While such pathways protect cancer cells from recognition by NK cells, they have the opposite effect on recognition by CD8 T cells.[14]

SPPL3 has been noted in other screens for sensitivity to cytotoxic T cells. Loss of *SPPL3* in the pre-B-ALL cell line NALM6 resulted in increased glycosylation of CD19 and a direct impairment of CAR-T cell effector function and a reduction in their anti-tumor efficacy.[26,43] Another study reported that the response of CD8 T cells to HLA class I was impaired in

SPPL3-knockout cells through a different pathway, which involves an increase of glycosphingolipids in antigen-presenting cells. The accumulation of glycosyltransferases, such as B3GNT5, in *SPPL3*-knockout cells increased the amount of glycosphingolipids at the plasma membrane, which sterically interfered with the accessibility of HLA class I to its receptors and diminished CD8+ T cell activation.[44]

Having identified SPPL3 as a major regulator of sensitivity to NK cells, we went on to determine how a higher abundance of membrane-tethered intracellular glycosyltransferases impacts glycosylation of cell-surface proteins and how this leads to target cell resistance. Was it mainly a quantitative effect due to higher numbers of glycosylated proteins and of glycosylation sites on proteins, or was it more specific, due to changes in the type of *N*-glycans? To address this, *SPPL3*-knockout cells were subjected to another round of selection by co-culture with NK cells. This time an sgRNA library focused on genes that control glycosylation pathways was used to identify the type of glycans that may be responsible for resistance to NK cells. Two independent screens with this library identified MGAT2, which adds GlcNAc on the second branch after the trimming of high-mannose precursors, and B3GNT2, a transferase specialized in the extension of branched *N*-glycans by adding GlcNAc in a β1,3 linkage to an unsialylated terminal galactose.[33] B3GNT2 has also been identified as a driver of resistance of human melanoma cells to T cell-mediated cytotoxicity.[45] Notably, *B3GNT2* ranks as one of the highly amplified genes in DLBCL patients, suggesting a potential alteration in glycosylation and immune evasion.[46] B3GNT2 prefers to elongate the fourth branch, which is added by MGAT5.[35,47] B3GNT2 competes with sialyltransferases for the same substrate, namely one of the four terminal Gal on tetra-antennary *N*-glycans. Sialyltransferases get a head start, as they sialylate any terminal Gal, including those on partially branched *N*-glycans, while B3GNT2 prefers tetra-antennary *N*-glycans. Remarkably, the resistance to NK-mediated lysis conferred by *SPPL3* knockout was further increased by deletion of *ST6GAL1* (Figures 6A and 6B). As ST6GAL1 specializes in α2,6-linked sialylation of terminal Gal on branched *N*-glycans,[48] its absence provides more opportunities for branch extension by B3GNT2.

In addition to *MGAT2*, the other three *MGAT* genes 1, 4, and 5 required for synthesis of tetra-antennary *N*-glycans were also detected in our screen, providing further evidence that high *N*-glycan branching contributes to the resistant phenotype. Expression of *MGAT5* has been linked to cancer[35,47,49] and inhibits killing of pancreatic adenocarcinoma by CAR-T cells targeting CD44.[50] In contrast to *MGAT2*, knockout of *MGAT3* conferred additional resistance against NK-mediated killing to *SPPL3*-knockout cells. MGAT3 transfers a GlcNAc in a β1,4 linkage to the core β-mannose of *N*-glycan, a step referred to as a bisecting GlcNAc. Addition of a bisecting GlcNAc inhibits further branching by MGAT4 and MGAT5.[34,35] Therefore, the absence of MGAT3 facilitates MGAT4- and MGAT5-mediated addition of the third and fourth *N*-glycan antennae, thereby increasing the number of substrates for B3GNT2-mediated elongation and the resistance of target cells to NK-mediated lysis.

N-Glycan species with LacNAc extensions identified by our glycomic analysis included four that carried one LacNAc and one each with extensions of two, four, and six LacNAc units, all of which were enriched in *SPPL3*-knockout cells. Our glycoproteomic analysis demonstrated the presence of tetra-antennary *N*-glycans that included at least one LacNAc extension. They were detected on abundant proteins only, such as CD48 and ICAM-1. These extended *N*-glycans were significantly enriched in *SPPL3*-knockout cells. As CD48 is the ligand of NK co-activation receptor 2B4, high branching and elongation of CD48 *N*-glycans could impair NK cytotoxicity toward adult T cell leukemia and lymphoma, which depends on CD48 expression.[51]

In this study, we demonstrate that SPPL3 functions as a primary determinant of interactions between NK cells and tumor cells, with profound implications for cancer biology. We identified the specific steps in the *N*-glycosylation pathway in target cells that contributed the most to resistance against NK cells, namely high branching of *N*-glycans that are further elongated by addition of LacNAc. Malignant B cells and other tumor cells that upregulate transferases in this pathway may acquire resistance against cytotoxic T cells and NK cells. Downregulation or mutations of the *SPPL3* gene can promote tumor cell escape due to intracellular accumulation of several glycosyltransferases.[38] Our study supports the feasibility of incorporating glycosylation pathway inhibitors into cancer treatment regimens to further enhance the efficacy of cancer therapy. Moreover, CAR-T and CAR-NK cells are at the forefront of cancer immunotherapy, and their effectiveness relies on specific recognition of tumor cell antigens. In this regard, a major concern is the diminished binding of tumor-specific antibodies in the context of monoclonal antibody therapies and scFvs built into CARs. It is therefore critical to identify antibody epitopes that are not shielded by large glycans on tumor antigens to ensure the targeted destruction of tumor cells by monoclonal antibody and CAR therapies.

Limitations of the study

SPPL3 is one of several genes that regulate target cell sensitivity to NK cells. Other genes that confer sensitivity, such as *FBXO11* identified here, deserve our attention. Our *N*-glycan analysis demonstrated that *SPPL3*-knockout cells have a greater abundance of complex, tetra-antennary glycans extended by one or more LacNAc. Proteins bearing such *N*-glycans were detected in the glycoproteomic analysis of *SPPL3*-knockout cells, such as ICAM-1 and CD48. However, the detection limit was not sufficient to collect information on less abundant proteins of interest, such as CD58, MICB, and CD20. Nevertheless, complex glycosylation of CD58 was confirmed by biochemical analysis. Ultimately, *in vivo* models and clinical samples of cancer patients will have to be used to determine the impact of deregulation of protein glycosylation pathways on patient survival.

STAR★METHODS

Detailed methods are provided in the online version of this paper and include the following:

- KEY RESOURCES TABLE
- RESOURCE AVAILABILITY
  - Lead contact
  - Materials availability

AUTHOR CONTRIBUTIONS

X.Z. and E.O.L. conceived the project. X.Z., J.W., Y.J. and S.R. performed the experiments. X.Z., M.V., and K.-T.P. provided the methodology for performing the experiments. X.Z., Y.J., Z.A.C., and K.-T.P. contributed formal analysis. X.Z. and E.O.L. wrote the manuscript. X.Z., E.O.L., M.V., F.M., J.W., Y.J., S.R., and S.S. wrote and edited the manuscript. E.O.L. and K.-T.P. supervised the study. E.O.L., L.M.S., H.U., and K.-T.P. acquired funding.

DECLARATION OF INTERESTS

The authors declare no competing interests.

REFERENCES

1. Long, E.O., Kim, H.S., Liu, D., Peterson, M.E., and Rajagopalan, S. (2013). Controlling natural killer cell responses: integration of signals for activation and inhibition. Annu. Rev. Immunol. 31, 227–258. https://doi.org/10.1146/annurev-immunol-020711-075005.

2. Myers, J.A., and Miller, J.S. (2021). Exploring the NK cell platform for cancer immunotherapy. Nat. Rev. Clin. Oncol. 18, 85–100. https://doi.org/10.1038/s41571-020-0426-7.

3. Morvan, M.G., and Lanier, L.L. (2016). NK cells and cancer: you can teach innate cells new tricks. Nat. Rev. Cancer 16, 7–19. https://doi.org/10.1038/nrc.2015.5.

4. Chiossone, L., Dumas, P.Y., Vienne, M., and Vivier, E. (2018). Natural killer cells and other innate lymphoid cells in cancer. Nat. Rev. Immunol. 18, 671–688. https://doi.org/10.1038/s41577-018-0061-z.

5. Barry, K.C., Hsu, J., Broz, M.L., Cueto, F.J., Binnewies, M., Combes, A.J., Nelson, A.E., Loo, K., Kumar, R., Rosenblum, M.D., et al. (2018). A natural killer-dendritic cell axis defines checkpoint therapy-responsive tumor microenvironments. Nat. Med. 24, 1178–1191. https://doi.org/10.1038/s41591-018-0085-8.

6. Böttcher, J.P., Bonavita, E., Chakravarty, P., Blees, H., Cabeza-Cabrerizo, M., Sammicheli, S., Rogers, N.C., Sahai, E., Zelenay, S., and Reis e Sousa, C. (2018). NK Cells Stimulate Recruitment of cDC1 into the Tumor Microenvironment Promoting Cancer Immune Control. Cell 172, 1022–1037.e14. https://doi.org/10.1016/j.cell.2018.01.004.

7. Souza-Fonseca-Guimaraes, F., Cursons, J., and Huntington, N.D. (2019). The Emergence of Natural Killer Cells as a Major Target in Cancer Immunotherapy. Trends Immunol. 40, 142–158. https://doi.org/10.1016/j.it.2018.12.003.

8. Liu, E., Marin, D., Banerjee, P., Macapinlac, H.A., Thompson, P., Basar, R., Nassif Kerbauy, L., Overman, B., Thall, P., Kaplan, M., et al. (2020). Use of CAR-Transduced Natural Killer Cells in CD19-Positive Lymphoid Tumors. N. Engl. J. Med. 382, 545–553. https://doi.org/10.1056/NEJMoa1910607.

9. Huntington, N.D., Cursons, J., and Rautela, J. (2020). The cancer-natural killer cell immunity cycle. Nat. Rev. Cancer 20, 437–454. https://doi.org/10.1038/s41568-020-0272-z.

10. Zhuang, X., Veltri, D.P., and Long, E.O. (2019). Genome-Wide CRISPR Screen Reveals Cancer Cell Resistance to NK Cells Induced by NK-Derived IFN-gamma. Front. Immunol. 10, 2879. https://doi.org/10.3389/fimmu.2019.02879.

11. Dubrot, J., Du, P.P., Lane-Reticker, S.K., Kessler, E.A., Muscato, A.J., Mehta, A., Freeman, S.S., Allen, P.M., Olander, K.E., Ockerman, K.M., et al. (2022). In vivo CRISPR screens reveal the landscape of immune evasion pathways across cancer. Nat. Immunol. 23, 1495–1506. https://doi.org/10.1038/s41590-022-01315-x.

12. Freeman, A.J., Vervoort, S.J., Ramsbottom, K.M., Kelly, M.J., Michie, J., Pijpers, L., Johnstone, R.W., Kearney, C.J., and Oliaro, J. (2019). Natural Killer Cells Suppress T Cell-Associated Tumor Immune Evasion. Cell Rep. 28, 2784–2794.e5. https://doi.org/10.1016/j.celrep.2019.08.017.

13. Sheffer, M., Lowry, E., Beelen, N., Borah, M., Amara, S.N.A., Mader, C.C., Roth, J.A., Tsherniak, A., Freeman, S.S., Dashevsky, O., et al. (2021). Genome-scale screens identify factors regulating tumor cell responses to natural killer cells. Nat. Genet. 53, 1196–1206. https://doi.org/10.1038/s41588-021-00889-w.

14. Patel, S.J., Sanjana, N.E., Kishton, R.J., Eidizadeh, A., Vodnala, S.K., Cam, M., Gartner, J.J., Jia, L., Steinberg, S.M., Yamamoto, T.N., et al. (2017). Identification of essential genes for cancer immunotherapy. Nature 548, 537–542. https://doi.org/10.1038/nature23477.

15. Challa-Malladi, M., Lieu, Y.K., Califano, O., Holmes, A.B., Bhagat, G., Murty, V.V., Dominguez-Sola, D., Pasqualucci, L., and Dalla-Favera, R. (2011). Combined genetic inactivation of beta2-Microglobulin and CD58 reveals frequent escape from immune recognition in diffuse large B cell lymphoma. Cancer Cell 20, 728–740. https://doi.org/10.1016/j.ccr.2011.11.006.

16. Klanova, M., Oestergaard, M.Z., Trněný, M., Hiddemann, W., Marcus, R., Sehn, L.H., Vitolo, U., Bazeos, A., Goede, V., Zeuner, H., et al. (2019). Prognostic Impact of Natural Killer Cell Count in Follicular Lymphoma and Diffuse Large B-cell Lymphoma Patients Treated with Immunochemotherapy. Clin. Cancer Res. 25, 4634–4643. https://doi.org/10.1158/1078-0432.CCR-18-3270.

17. Shimizu, Y., Geraghty, D.E., Koller, B.H., Orr, H.T., and DeMars, R. (1988). Transfer and expression of three cloned human non-HLA-A,B,C class I major histocompatibility complex genes in mutant lymphoblastoid cells. Proc. Natl. Acad. Sci. USA *85*, 227–231. https://doi.org/10.1073/pnas.85.1.227.

18. Dervovic, D., Malik, A.A., Chen, E.L.Y., Narimatsu, M., Adler, N., Afiuni-Zadeh, S., Krenbek, D., Martinez, S., Tsai, R., Boucher, J., et al. (2023). In vivo CRISPR screens reveal Serpinb9 and Adam2 as regulators of immune therapy response in lung cancer. Nat. Commun. *14*, 3150. https://doi.org/10.1038/s41467-023-38841-7.

19. Wang, W., Wu, S., Cen, Z., Zhang, Y., Chen, Y., Huang, Y., Cillo, A.R., Prokopec, J.S., Quarato, G., Vignali, D.A.A., et al. (2022). Mobilizing phospholipids on tumor plasma membrane implicates phosphatidylserine externalization blockade for cancer immunotherapy. Cell Rep. *41*, 111582. https://doi.org/10.1016/j.celrep.2022.111582.

20. Bryceson, Y.T., March, M.E., Ljunggren, H.G., and Long, E.O. (2006). Synergy among receptors on resting NK cells for the activation of natural cytotoxicity and cytokine secretion. Blood *107*, 159–166. https://doi.org/10.1182/blood-2005-04-1351.

21. Bryceson, Y.T., Ljunggren, H.G., and Long, E.O. (2009). Minimal requirement for induction of natural cytotoxicity and intersection of activation signals by inhibitory receptors. Blood *114*, 2657–2666. https://doi.org/10.1182/blood-2009-01-201632.

22. Duan, S., Cermak, L., Pagan, J.K., Rossi, M., Martinengo, C., di Celle, P.F., Chapuy, B., Shipp, M., Chiarle, R., and Pagano, M. (2012). FBXO11 targets BCL6 for degradation and is inactivated in diffuse large B-cell lymphomas. Nature *481*, 90–93. https://doi.org/10.1038/nature10688.

23. Kasuga, Y., Ouda, R., Watanabe, M., Sun, X., Kimura, M., Hatakeyama, S., and Kobayashi, K.S. (2023). FBXO11 constitutes a major negative regulator of MHC class II through ubiquitin-dependent proteasomal degradation of CIITA. Proc. Natl. Acad. Sci. USA *120*, e2218955120. https://doi.org/10.1073/pnas.2218955120.

24. Saito, M., Novak, U., Piovan, E., Basso, K., Sumazin, P., Schneider, C., Crespo, M., Shen, Q., Bhagat, G., Califano, A., et al. (2009). BCL6 suppression of BCL2 via Miz1 and its disruption in diffuse large B cell lymphoma. Proc. Natl. Acad. Sci. USA *106*, 11294–11299. https://doi.org/10.1073/pnas.0903854106.

25. Masternak, K., Peyraud, N., Krawczyk, M., Barras, E., and Reith, W. (2003). Chromatin remodeling and extragenic transcription at the MHC class II locus control region. Nat. Immunol. *4*, 132–137. https://doi.org/10.1038/ni883.

26. Dufva, O., Koski, J., Maliniemi, P., Ianevski, A., Klievink, J., Leitner, J., Pölönen, P., Hohtari, H., Saeed, K., Hannunen, T., et al. (2020). Integrated drug profiling and CRISPR screening identify essential pathways for CAR T-cell cytotoxicity. Blood *135*, 597–609. https://doi.org/10.1182/blood.2019002121.

27. Dufva, O., Gandolfi, S., Huuhtanen, J., Dashevsky, O., Duàn, H., Saeed, K., Klievink, J., Nygren, P., Bouhlal, J., Lahtela, J., et al. (2023). Single-cell functional genomics reveals determinants of sensitivity and resistance to natural killer cells in blood cancers. Immunity *56*, 2816–2835.e13. https://doi.org/10.1016/j.immuni.2023.11.008.

28. Kuhn, P.H., Voss, M., Haug-Kröper, M., Schröder, B., Schepers, U., Bräse, S., Haass, C., Lichtenthaler, S.F., and Fluhrer, R. (2015). Secretome analysis identifies novel signal Peptide peptidase-like 3 (Sppl3) substrates and reveals a role of Sppl3 in multiple Golgi glycosylation pathways. Mol. Cell. Proteomics *14*, 1584–1598. https://doi.org/10.1074/mcp.M115.048298.

29. Voss, M., Künzel, U., Higel, F., Kuhn, P.H., Colombo, A., Fukumori, A., Haug-Kröper, M., Klier, B., Grammer, G., Seidl, A., et al. (2014). Shedding of glycan-modifying enzymes by signal peptide peptidase-like 3 (SPPL3) regulates cellular N-glycosylation. EMBO J. *33*, 2890–2905. https://doi.org/10.15252/embj.201488375.

30. Grier, J.T., Forbes, L.R., Monaco-Shawver, L., Oshinsky, J., Atkinson, T.P., Moody, C., Pandey, R., Campbell, K.S., and Orange, J.S. (2012). Human immunodeficiency-causing mutation defines CD16 in spontaneous NK cell cytotoxicity. J. Clin. Invest. *122*, 3769–3780. https://doi.org/10.1172/JCI64837.

31. Batlevi, C.L., Matsuki, E., Brentjens, R.J., and Younes, A. (2016). Novel immunotherapies in lymphoid malignancies. Nat. Rev. Clin. Oncol. *13*, 25–40. https://doi.org/10.1038/nrclinonc.2015.187.

32. Zhu, Y., Groth, T., Kelkar, A., Zhou, Y., and Neelamegham, S. (2021). A GlycoGene CRISPR-Cas9 lentiviral library to study lectin binding and human glycan biosynthesis pathways. Glycobiology *31*, 173–180. https://doi.org/10.1093/glycob/cwaa074.

33. Kadirvelraj, R., Yang, J.Y., Kim, H.W., Sanders, J.H., Moremen, K.W., and Wood, Z.A. (2021). Comparison of human poly-N-acetyl-lactosamine synthase structure with GT-A fold glycosyltransferases supports a modular assembly of catalytic subsites. J. Biol. Chem. *296*, 100110. https://doi.org/10.1074/jbc.RA120.015305.

34. Nakano, M., Mishra, S.K., Tokoro, Y., Sato, K., Nakajima, K., Yamaguchi, Y., Taniguchi, N., and Kizuka, Y. (2019). Bisecting GlcNAc Is a General Suppressor of Terminal Modification of N-glycan. Mol. Cell. Proteomics *18*, 2044–2057. https://doi.org/10.1074/mcp.RA119.001534.

35. Taniguchi, N., and Kizuka, Y. (2015). Glycans and cancer: role of N-glycans in cancer biomarker, progression and metastasis, and therapeutics. Adv. Cancer Res. *126*, 11–51. https://doi.org/10.1016/bs.acr.2014.11.001.

36. Truberg, J., Hobohm, L., Jochimsen, A., Desel, C., Schweizer, M., and Voss, M. (2022). Endogenous tagging reveals a mid-Golgi localization of the glycosyltransferase-cleaving intramembrane protease SPPL3. Biochim. Biophys. Acta. Mol. Cell Res. *1869*, 119345. https://doi.org/10.1016/j.bbamcr.2022.119345.

37. Zhai, H. (2022). Investigating the role of genomic alterations and altered DNA replication timing during malignant transformation in tumours. Doctor of Philosophy Thesis (Doctoral) (University College London).

38. Bentham, R., Litchfield, K., Watkins, T.B.K., Lim, E.L., Rosenthal, R., Martínez-Ruiz, C., Hiley, C.T., Bakir, M.A., Salgado, R., Moore, D.A., et al. (2021). Using DNA sequencing data to quantify T cell fraction and therapy response. Nature *597*, 555–560. https://doi.org/10.1038/s41586-021-03894-5.

39. Prager, I., Liesche, C., van Ooijen, H., Urlaub, D., Verron, Q., Sandström, N., Fasbender, F., Claus, M., Eils, R., Beaudouin, J., et al. (2019). NK cells switch from granzyme B to death receptor-mediated cytotoxicity during serial killing. J. Exp. Med. *216*, 2113–2127. https://doi.org/10.1084/jem.20181454.

40. Anczuków, O., Rosenberg, A.Z., Akerman, M., Das, S., Zhan, L., Karni, R., Muthuswamy, S.K., and Krainer, A.R. (2012). The splicing factor SRSF1 regulates apoptosis and proliferation to promote mammary epithelial cell transformation. Nat. Struct. Mol. Biol. *19*, 220–228. https://doi.org/10.1038/nsmb.2207.

41. Kędzierska, H., and Piekiełko-Witkowska, A. (2017). Splicing factors of SR and hnRNP families as regulators of apoptosis in cancer. Cancer Lett. *396*, 53–65. https://doi.org/10.1016/j.canlet.2017.03.013.

42. Kearney, C.J., Vervoort, S.J., Hogg, S.J., Ramsbottom, K.M., Freeman, A.J., Lalaoui, N., Pijpers, L., Michie, J., Brown, K.K., Knight, D.A., et al. (2018). Tumor immune evasion arises through loss of TNF sensitivity. Sci. Immunol. *3*, eaar3451. https://doi.org/10.1126/sciimmunol.aar3451.

43. Heard, A., Landmann, J.H., Hansen, A.R., Papadopoulou, A., Hsu, Y.S., Selli, M.E., Warrington, J.M., Lattin, J., Chang, J., Ha, H., et al. (2022). Antigen glycosylation regulates efficacy of CAR T cells targeting CD19. Nat. Commun. *13*, 3367. https://doi.org/10.1038/s41467-022-31035-7.

44. Jongsma, M.L.M., de Waard, A.A., Raaben, M., Zhang, T., Cabukusta, B., Platzer, R., Blomen, V.A., Xagara, A., Verkerk, T., Bliss, S., et al. (2021). The SPPL3-defined glycosphingolipid repertoire orchestrates HLA class I-mediated immune responses. Immunity *54*, 387. https://doi.org/10.1016/j.immuni.2021.01.016.

45. Joung, J., Kirchgatterer, P.C., Singh, A., Cho, J.H., Nety, S.P., Larson, R.C., Macrae, R.K., Deasy, R., Tseng, Y.Y., Maus, M.V., and Zhang, F.

(2022). CRISPR activation screen identifies BCL-2 proteins and B3GNT2 as drivers of cancer resistance to T cell-mediated cytotoxicity. Nat. Commun. *13*, 1606. https://doi.org/10.1038/s41467-022-29205-8.

46. Dersh, D., Phelan, J.D., Gumina, M.E., Wang, B., Arbuckle, J.H., Holly, J., Kishton, R.J., Markowitz, T.E., Seedhom, M.O., Fridlyand, N., et al. (2021). Genome-wide Screens Identify Lineage- and Tumor-Specific Genes Modulating MHC-I- and MHC-II-Restricted Immunosurveillance of Human Lymphomas. Immunity *54*, 116–131.e10. https://doi.org/10.1016/j.immuni.2020.11.002.

47. Lau, K.S., and Dennis, J.W. (2008). N-Glycans in cancer progression. Glycobiology *18*, 750–760. https://doi.org/10.1093/glycob/cwn071.

48. Hugonnet, M., Singh, P., Haas, Q., and von Gunten, S. (2021). The Distinct Roles of Sialyltransferases in Cancer Biology and Onco-Immunology. Front. Immunol. *12*, 799861. https://doi.org/10.3389/fimmu.2021.799861.

49. de-Souza-Ferreira, M., Ferreira, É.E., and de-Freitas-Junior, J.C.M. (2023). Aberrant N-glycosylation in cancer: MGAT5 and beta1,6-GlcNAc branched N-glycans as critical regulators of tumor development and progression. Cell. Oncol. *46*, 481–501. https://doi.org/10.1007/s13402-023-00770-4.

50. Greco, B., Malacarne, V., De Girardi, F., Scotti, G.M., Manfredi, F., Angelino, E., Sirini, C., Camisa, B., Falcone, L., Moresco, M.A., et al. (2022). Disrupting N-glycan expression on tumor cells boosts chimeric antigen receptor T cell efficacy against solid malignancies. Sci. Transl. Med. *14*, eabg3072. https://doi.org/10.1126/scitranslmed.abg3072.

51. Chiba, M., Shimono, J., Ishio, T., Takei, N., Kasahara, K., Ogasawara, R., Ara, T., Goto, H., Izumiyama, K., Otsuguro, S., et al. (2022). Genome-wide CRISPR screens identify CD48 defining susceptibility to NK cytotoxicity in peripheral T-cell lymphomas. Blood *140*, 1951–1963. https://doi.org/10.1182/blood.2022015646.

52. Sanjana, N.E., Shalem, O., and Zhang, F. (2014). Improved vectors and genome-wide libraries for CRISPR screening. Nat Methods *11*, 783–784. https://doi.org/10.1038/nmeth.3047.

53. Robinson, M.D., McCarthy, D.J., and Smyth, G.K. (2010). edgeR: a Bioconductor package for differential expression analysis of digital gene expression data. Bioinformatics *26*, 139–140. https://doi.org/10.1093/bioinformatics/btp616.

54. Li, W., Köster, J., Xu, H., Chen, C.H., Xiao, T., Liu, J.S., Brown, M., and Liu, X.S. (2015). Quality control, modeling, and visualization of CRISPR screens with MAGeCK-VISPR. Genome Biol. *16*, 281. https://doi.org/10.1186/s13059-015-0843-6.

55. Perez-Riverol, Y., Bai, J., Bandla, C., García-Seisdedos, D., Hewapathirana, S., Kamatchinathan, S., Kundu, D.J., Prakash, A., Frericks-Zipper, A., Eisenacher, M., et al. (2022). The PRIDE database resources in 2022: a hub for mass spectrometry-based proteomics evidences. Nucleic Acids Res. *50*, D543–D552. https://doi.org/10.1093/nar/gkab1038.

56. Phelan, J.D., Young, R.M., Webster, D.E., Roulland, S., Wright, G.W., Kasbekar, M., Shaffer, A.L., 3rd, Ceribelli, M., Wang, J.Q., Schmitz, R., et al. (2018). A multiprotein supercomplex controlling oncogenic signalling in lymphoma. Nature *560*, 387–391. https://doi.org/10.1038/s41586-018-0290-0.

57. Choi, J., Phelan, J.D., Wright, G.W., Häupl, B., Huang, D.W., Shaffer, A.L., 3rd, Young, R.M., Wang, Z., Zhao, H., Yu, X., et al. (2020). Regulation of B cell receptor-dependent NF-kappaB signaling by the tumor suppressor KLHL14. Proc. Natl. Acad. Sci. USA *117*, 6092–6102. https://doi.org/10.1073/pnas.1921187117.

58. Joung, J., Konermann, S., Gootenberg, J.S., Abudayyeh, O.O., Platt, R.J., Brigham, M.D., Sanjana, N.E., and Zhang, F. (2017). Genome-scale CRISPR-Cas9 knockout and transcriptional activation screening. Nat. Protoc. *12*, 828–863. https://doi.org/10.1038/nprot.2017.016.

59. Hobohm, L., Koudelka, T., Bahr, F.H., Truberg, J., Kapell, S., Schacht, S.S., Meisinger, D., Mengel, M., Jochimsen, A., Hofmann, A., et al. (2022). N-terminome analyses underscore the prevalence of SPPL3-mediated intramembrane proteolysis among Golgi-resident enzymes and its role in Golgi enzyme secretion. Cell. Mol. Life Sci. *79*, 185. https://doi.org/10.1007/s00018-022-04163-y.

60. Fang, P., Ji, Y., Silbern, I., Doebele, C., Ninov, M., Lenz, C., Oellerich, T., Pan, K.T., and Urlaub, H. (2020). A streamlined pipeline for multiplexed quantitative site-specific N-glycoproteomics. Nat. Commun. *11*, 5268. https://doi.org/10.1038/s41467-020-19052-w.

61. Shajahan, A., Heiss, C., Ishihara, M., and Azadi, P. (2017). Glycomic and glycoproteomic analysis of glycoproteins-a tutorial. Anal. Bioanal. Chem. *409*, 4483–4505. https://doi.org/10.1007/s00216-017-0406-7.

STAR★METHODS

KEY RESOURCES TABLE

REAGENT or RESOURCE	SOURCE	IDENTIFIER
Antibodies		
Anti-human CD107a FITC	BD Biosciences	555800, clone H4A3; RRID: AB_396134
Anti-human CD56 BV421	BD Biosciences	562751, clone NCAM16.2; RRID: AB_2732054
Anti-human SPPL3	Millipore Sigma	MABS1910, clone 7F9
Anti-human FBXO11 polyclonal	NOVUS	NB100-59826; RRID: AB_892469
Anti-human CD58	BD Biosciences	555919, clone 1C3; RRID: AB_396220
Anti-human CD58 PE	BD Biosciences	555921, clone 1C3; RRID: AB_2076117
Anti-human MICB PE	R&D Systems	FAB1599P, clone 236511; RRID: AB_10972308
Anti-human MICB polyclonal	R&D Systems	AF1599; RRID: AB_354884
Anti-human TRAIL-R1 PE	BD Biosciences	564180, clone S35-934; RRID: AB_2738648
Anti-human TRAIL-R2 PE	BD Biosciences	565499, clone YM366; RRID: AB_2732871
Anti-human CD48 PE	BD Biosciences	552855, clone TU145; RRID: AB_394496
Anti-human ICAM1	BD Biosciences	555511, clone HA58; RRID: AB_395901
Anti-human HLA-E	BioLegend	342604, clone 3D12; RRID: AB_1659250
Anti-human MGAT5	R&D Systems	MAB5469, clone 706824; RRID: AB_10972310
Anti-human actin	Santa Cruz	sc-8432, clone C-2; RRID: AB_626630
Anti-HA high affinity	Millipore Sigma	11867423001, clone 3F10; RRID: AB_390918
Bacterial and virus strains		
Stellar *E. coli* HST08 competent cells	TakaRa	636763
Endura *E. coli* Electrocompetent Cells	Biosearch Technologies	F861214
Biological samples		
Human Leukopak (for NK cell isolation)	NIH blood bank	NA
Chemicals, peptides, and recombinant proteins		
Kifunensine	Millipore Sigma	K1140
Swainsonine	Millipore Sigma	S8195
Concanavalin A (Con A), FITC	Vector labs	FL-1001-25
Sambucus Nigra Lectin (SNA), FITC	Vector labs	FL-1301-2
Phaseolus Vulgaris Erythroagglutinin (PHA-E), FITC	Vector labs	FL-1121-2
Lycopersicon esculentum Lectin (LEL), FITC	Vector labs	FL-1171-1
Human CD2 Fc Chimera Protein	R&D Systems	1856-CD
Human NKG2D Fc Chimera Protein	R&D Systems	1299-NK-050
Recombinant Human IgG1 Fc Protein	R&D systems	110-HG-100
Critical commercial assays		
123count eBeads™	ThermoFisher	01-1234-42
Dead Cell Removal Kit	Miltenyi Biotec	130-090-101
In-Fusion Snap Assembly Bundle	TaKaRa	638945
EasySep Human NK Cell Enrichment Kit	STEMCELL Technologies	19055
EasySep™ Human CD56 Positive Selection Kit	STEMCELL Technologies	17855
PKH67 Green Fluorescent Cell Linker Kit	SIGMA	PKH67GL
NEBNext® High-Fidelity 2X PCR Master Mix	New England Biolabs	M0541L
Deposited data		
Raw and analyzed CRISPR screen and RNA-seq data	This paper	GEO: GSE228188, Table S2
Glycoproteomics data	This paper	PRIDE: PXD040769, Tables S1 and S2

Continued		
REAGENT or RESOURCE	SOURCE	IDENTIFIER
Source data	This paper	Table S3
Experimental models: Cell lines		
LCL 721.221 cell line	Lab of Robert DeMars	CelloSaurus, RRID: CVCL_6263
RIVA cell line	Lab of Martin Dyer	CelloSaurus, RRID: CVCL_1885
OCI-LY1 cell line	Lab of Hans Messner	CelloSaurus, RRID: CVCL_1879
WSU-NHL cell line	DSMZ	CelloSaurus, RRID: CVCL_1793
Lenti-X 293T	TaKaRa	632180
Oligonucleotides		
sgSPPL3-1 (CTTGTTAAATACTGGCACAT)	GeCKO V2 library	Addgene library # 1000000049
sgSPPL3-2 (CGAGTAGGTCTGCTCCGCCA)	GeCKO V2 library	Addgene library # 1000000049
sgFBXO11 (ACTTCAACTACAGAAAACTT)	GeCKO V2 library	Addgene library # 1000000049
sgNT (TCCTGCCAAGAAACACCCTT)	GeCKO V2 library	Addgene library # 1000000049
sgMICB (CACCTGCAGCGAGGTCTCAG)	GeCKO V2 library	Addgene library # 1000000049
sgCD58 (CATGTTGTAATTACTGCTAA)	GeCKO V2 library	Addgene library # 1000000049
sgTNFRSF10B (ACACATTCGATGTCACTCCA)	GeCKO V2 library	Addgene library # 1000000049
sgTNFRSF10A (ACACACTCGATGTCACTCCA)	GeCKO V2 library	Addgene library # 1000000049
sgB2M (ACCGCGTGAGTAAACCTGAATCTT)	GeCKO V2 library	Addgene library # 1000000049
sgB3GNT2 (GTTCCTCTACTCCGGCCACC)	GeCKO V2 library	Addgene library # 1000000049
Recombinant DNA		
GeCKO V2 human CRISPR knockout library	Sanjana et al.[52]	Addgene library # 1000000049
Human GlycoGene CRISPR pooled library	Zhu et al.[32]	Addgene library #140961
LentiGuide-Puro vector	Sanjana et al.[52]	Addgene plasmid #52963
Software and algorithms		
edgeR	Robinson et al.[53]	https://bioconductor.org/packages/release/bioc/html/edgeR.html
MAGeCK	Li et al.[54]	https://sourceforge.net/p/mageck/wiki/Home/

RESOURCE AVAILABILITY

Lead contact
Additional information and requests for resources should be directed to the lead contact, Eric O. Long (elong@nih.gov).

Materials availability
All materials generated in this study will be made available upon reasonable request.

Data and code availability
- All data reported in this paper will be shared by the lead contact upon request. CRISPR screen and RNA-seq data in this paper are available at GEO under the accession number GSE228188. Datasets GSM7116256-GSM7116259 are related to Figures 1C–1F, S1D, and S1E. Datasets GSM7116260-GSM7116267 are related to Figures 6A and 6B. Datasets GSM7116268-GSM7116273 are related to Figures S2C–S2E. A sample information list has been included (Table S2). The mass spectrometry-based glycoproteomics data has been deposited to the ProteomeXchange Consortium via the PRIDE[55] partner repository with the dataset identifier PXD040769. A sample information list has been included (Table S2), with biological replicates representing two individual TMT6 labeling experiments. To enhance identification depth, the samples were first combined and then underwent separation into six fractions using basic reverse-phase fractionation technology before mass spec analysis. In each fractionation, the sgNT 221 sample is assigned to channel 1, while the sgSPPL3 sample is assigned to channel 2. All the datasets related to Figures 7B–7E are listed in Table S2. All source data are available in Table S3.
- This paper does not report original code.
- Additional information required to reanalyze the data reported in this paper is available from the lead contact upon request.

EXPERIMENTAL MODEL AND STUDY PARTICIPANT DETAILS

Cells

Peripheral blood samples from healthy US adults were obtained from the NIH Department of Transfusion Medicine under an NIH Institutional Review Board-approved protocol (99-CC-0168) with informed consent. NK cells were isolated using negative selection (Stemcell Technologies). The NK cells were then suspended in IMDM (Gibco) containing 10% human serum (Valley Biomedical) and were used within 4 days. To generate IL-2-activated NK cells, the freshly isolated NK cells were cultured together with irradiated autologous feeder cells in the presence of 10% purified IL-2 (Hemagen), 100 units/mL recombinant IL-2 (Roche), and 5 μg/mL PHA (Sigma), all in OpTimizer (Invitrogen) medium. Subsequently, expansion was carried out in the same medium, but without the PHA and feeder cells. 221 cells were cultured in RPMI 1640 medium (Gibco) with the addition of 10% heat-inactivated fetal calf serum (Gibco) and 2 mM L-Glutamine (Gibco). To block the glycosylation pathway, cells were either treated with 4 μg/mL kifunensine or 10 μg/mL swainsonine for 24 h before lectin staining or functional assays. RIVA, OCI-LY1, WSU-FSCCL cells were cultured in advanced RPMI-1640 medium (Gibco) with the addition of 5% heat-inactivated fetal calf serum (Gibco) and Penicillin-Streptomycin-Glutamine (100 X, Gibco). RIVA, OCI-LY1, or WSU-FSCCL cells expressing doxycycline-inducible Cas-9[56] were infected with lentiviruses encoding gRNAs targeting *B2M* in the pLKO-Neo-BFP vector and selected by neomycin as described previously.[57] Cells were then transduced with sgNT (in pLKO-Neo-BFP vector) or sgSPPL3 (in LentiGuide-puro vector) and selected by puromycin. Cells were cultured in medium supplemented with 200 μg/mL doxycycline (Sigma-Aldrich) for 10 days before using for killing assays.

METHOD DETAILS

Plasmids and lentivirus production

The sgRNAs that targeted specific genes were synthesized by Integrated DNA Technologies (IDT) and cloned into the BsmBI restriction sites of the LentiGuide-Puro vector using the In-Fusion cloning kit (TaKaRa) and transformed into Stellar *E. coli* competent cells (TaKaRa). To make SPPL3 and B3GNT2 double knockout cells, sgSPPL3-1 was cloned into a LentiGuide-hygro vector, which was modified from the LentiGudie-Puro vector by replace the puromycin-resistant gene with a hygromycin-resistant gene using the In-Fusion cloning kit. To prepare for lentivirus production, low-passage Lenti-X 293T cells (Clontech) were seeded into a T75 flask and transfected the following day using PEI Max (Polyethylenimine). The transfection procedure involved mixing 1.2 μg of pMD2.G plasmid, 2.3 μg of psPAX2 plasmid, 4.6 μg of LentiGuide-Puro plasmid, and 217 μL of serum-free DMEM in a Falcon tube. Then, 65 μL of PEI Max 40K (Polysciences) stock solution (1 mg/mL) was added and briefly vortexed. After 10 min, 8.6 mL of DMEM media containing 10% FCS was added to the tube. The culture medium for the 293T cells was replaced with the fresh medium containing the transfection mixture. Supernatants were collected two days after transfection, passed through a 0.45 μM filter, and stored at −80°C. The virus was either used directly or concentrated using PEG-it (System Biosciences) before use. To transduce human cell lines, the lentivirus was combined with polybrene to a final concentration of 8 μg/mL and added to the cells, which were then incubated for 2 days. The cells were subsequently centrifuged at 1200 rpm for 10 min and resuspended in complete medium with puromycin at pre-titrated concentrations.

Genome-wide CRISPR screen

The 221 cells were transduced with LentiBlast-Cas9 and selected by the addition of 10 μg/mL blasticidin. The GeCKO V2 human CRISPR knockout library from Addgene was then introduced into Endura Electrocompetent Cells by means of electroporation using a Bio-Rad Gene Pulser. The expanded CRISPR plasmid libraries were purified using Maxi-Prep and used to produce lentivirus. The lentivirus titer was determined using a previously described method.[58] The 221 cells that expressed Cas9 were transduced with the GeCKO V2 lentivirus library at a low multiplicity of infection (MOI) of 0.3 and selected with puromycin for 10 days. At least 180 x 10^{6} cells were used for transduction to ensure a coverage of >500 cells per sgRNA. The transduced 221 cells were selected and culture with 1 μg/mL puromycin for 10 days then incubated with IL-2-activated NK cells at a ratio of 1:5 to 1:10 and incubated for 48 to 72 h. The percentage of surviving 221 cells was monitored and, if necessary, additional NK cells were added until 10%–20% of the 221 cells remained. To recover the surviving 221 cells, the dead cells were first removed with a Dead Cell Removal Kit and then the NK cells were depleted using the EasySep Human CD56 Positive Selection Kit (Stemcell Technologies). The control 221 cells were kept in the same culture conditions but were not exposed to NK cells. The screen was performed with two biological repeats. The genomic DNA extraction and gRNA cassette amplification were carried out using a previously described method.[58] The amplified libraries were then multiplexed and analyzed on a NextSeq 500 with 75-bp single-end reads. The analysis of gRNA enrichment/depletion was performed using MAGeCK[54] MLE. This pipeline calculated the individual sgRNA read counts in libraries from both control and surviving 221 cells and then normalized the read counts of individual gRNAs based on non-targeting sgRNAs included in the library. The read counts of enriched gRNAs increased in surviving 221 cells compared to control 221 cells, while the read counts of depleted sgRNAs decreased in surviving 221 cells. MAGeCK utilizes a metric called the beta score to determine gene enrichment or depletion. A positive beta score indicates enrichment, while a negative beta score signifies depletion. The beta score of each gene is associated with the normalized log-fold change of all gRNAs targeting that gene. To create scatterplots, a randomized value was assigned to each gene to separate their labels in the plot, and the CRISPR beta score of each gene (y axis) was plotted against this randomized value (x axis).

Glycosylation-focused secondary CRISPR screen

To elucidate the specific glycan structure and transferase that responsible for the resistance caused by SPPL3-deletion, glycosylation focused CRISPR screens were conducted in sgNT or sgSPPL3 221 cells. Production of lentivirus from glycosylation-focused CRISPR library (glycoGene)[32] was described above. This glycoGene library consisted of 3637 sgRNAs targeting 347 genes involved in the glycosylation pathways. The library backbone constitutively expresses BFP for selection. SPPL3-deleted or sgNT 221 cells expressing LentiBlast-Cas9 were transduced with library virus at a low MOI of 0.3 for 2 days and cultured for an additional 2 days. At least 2×10^6 BFP positive 221 cells were sorted for each biological repeat to ensure coverage of >500 cells per sgRNA. Sorted cells were treated with doxycycline (dox) for 10 days to induce sgRNAs expression and genomic editing. Then, cells were co-incubated with NK cells at low E:T ratios and selected until 10%–20% of the 221 cells remained alive. Dead cells were removed with a Dead Cell Removal Kit (Miltenyi biotec). At least 4×10^6 million surviving cells were collected for DNA extractions and library amplification. Genomics DNA extractions were conducted using the PureLink Genomic DNA Mini Kit (Invitrogen). Library amplification was carried out by a two-step approach as described elsewhere.[32] Barcoded libraries were pooled and sequenced on an illumina MiSeq platform with 150 bp paired end reads.

Killing assay

The cytotoxicity assay was carried out using a flow cytometry-based approach. In brief, 221 cells were labeled with either PKH67-green or PKH26-red membrane dyes, then rinsed with complete growth medium. The IL-2-expanded NK cells were then combined with the pre-labeled 221 cells and incubated at 37°C in IMDM media supplemented with 10% FBS for overnight. The number of viable 221 cells was determined by counting beads using a flow cytometer. For ADCC assays, 221 cells were pre-incubated with 10 μg/mL rituximab for 15 min at room temperature before adding NK cells for lysis.

Degranulation assay

NK cells execute their function through secretion of lytic granules, which involves the fusion of the granule membrane with the cyto-plasmic membrane of the NK cell. This process leading to the surface exposure of lysosomal-associated proteins, including CD107a, typically found on the lipid bilayer surrounding lytic granules. Therefore, the membrane expression of CD107a serves as an indicator of NK cell activation and cytotoxic degranulation. Assessment of degranulation was performed using resting human NK cells. The target cells were combined with NK cells and incubated for 2 h at 37°C. The cells were then stained with Live/Dead-NIR (Thermo Fisher), anti-CD56-Bv421 (BD 562751), and anti-CD107a-FITC (BD 555800). Subsequently, flow cytometry was used to analyze the samples to identify NK cells that are CD107a positive.

Flow cytometry

For immune staining before flow cytometry, cells were incubated with premixed fluorophore-conjugated antibodies diluted in FCAS buffer (PBS, 0.5% BSA) at 4°C for 30 min. Cells were washed after staining and analyzed on an LSR II (BD Biosciences) or LSRFortessa X-20 (BD Biosciences). Data were analyzed with FlowJo (FlowJo, LLC). Lectin staining was employed to identify specific types of glycans in this study. ConA was used for high mannose, SNA for terminal sialic acid, PHA-E for complex *N*-glycan, and LEL for LacNAc. For lectin staining, cells were incubated with fluorophore-conjugated lectins, diluted in HBSS buffer (ThermoFisher Scientific), for 30 min at 4°C. Subsequently, the cells were washed and analyzed on a flow cytometer.

Western blot

To prepare samples for western blot, the cell pellets were resuspended in RIPA buffer containing 50 mM Tris-HCl (pH 8.0), 150 mM NaCl, 1.0% NP-40, 0.5% SDS, 0.5% sodium deoxycholate, cOmplete protease inhibitor cocktail (Roche), and PhosSTOP phospha-tase inhibitor cocktail (Millipore Sigma). The samples were then lysed on ice for 30 min and the cellular debris was removed by spin-ning at 12,000 rpm for 10 min. The protein lysates were mixed with 4X NuPAGE LDS-PAGE sample buffer (Invitrogen), separated on 4–12% Bis-Tris gels, transferred to PVDF membranes, and probed with the relevant antibodies. The chemiluminescent signal was detected using a ChemiDoc Imaging system (Bio-Rad).

To detect endogenous SPPL3 by western blot, a membrane extraction procedure was carried out.[59] Briefly, cells were resus-pended in hypotonic buffer kept at 4°C and sheared using a needle. The nuclei were sedimented by centrifugation at 2400*g* for 5 min at 4°C, and the resulting membrane pellets were obtained by centrifugation at 21,000g or 100,000g. The membrane pellets were then washed twice with carbonate buffer (0.1 M Na$_2$CO$_3$, 1 mM EDTA, pH 11.3), followed by washing with STE buffer (150 mM NaCl, 50 mM Tris, 2 mM EDTA, pH 7.6). Finally, membrane pellets were lysed in RIPA buffer and analyzed by western blot.

RNA-seq and data analysis

Cells were harvested in Trizol and combined with 200μL of 1-Bromo-3-chloropropane (Millipore Sigma), mixed vigorously, and centri-fuged at 16,000 x g for 15 min at 4°C. RNA containing aqueous phase (600 μL) was collected and passed through QiaShredder col-umn (Qiagen, Valencia, CA) at 21,000 x g for 2 min to homogenize any remaining genomic DNA in the aqueous phase. Aqueous phase was combined with 600uL of RLT lysis buffer (Qiagen, Valencia, CA) with 1% beta mercaptoethanol (MilliporeSigma, St. Louis, MO) and RNA was extracted using Qiagen AllPrep DNA/RNA 96 kit (Valencia, CA). An additional on-column DNase I treatment was per-formed during RNA extraction. All sample processing was performed using amplicon-free reagents and tools in aerosol-resistant

vials. RNA quality was analyzed using Agilent 2100 Bioanalyzer (Agilent Technologies, Santa Clara, CA). RNA samples were quantitated individually using a Qubit RNA High Sensitivity assay (Thermofisher, Waltham, MA) to create 1 μg aliquots for each. Samples were then processed using Truseq Stranded mRNA Library preparation kit (Illumina Inc., San Diego, CA) and single-end indexed for multiplexing. The resulting libraries were titrated using Kapa Library Quantification kit (Universal) (Roche, Basel, Switzerland) and measured on a Touch96 RTPCR instrument (Bio-Rad Laboratories, Hercules, CA). The samples were diluted to 2 nM working stocks and pooled together for sequencing on Illumina NextSeq MID-Output runs for 75 cycles in both directions and an additional 6 cycles to read the index. RNA-seq reads were compiled and filtered to remove any reads with PHRED scores less than 10 and aligned to the human hg38 genome using bowtie2. FeatureCounts was used to determine reads for annotated genes, and differential expression analysis was conducted using edgeR. Significantly differentially expressed genes, identified at an FDR of less than 5%, were categorized as upregulated or downregulated in the MD plot. Normalized counts per million (CPM) of genes encoding ligands for NK receptors were called out and shown as boxplots to compare their expression in sgSPPL3 and sgNT 221 cells.

N-glycoproteomic sample preparation, MS analysis and database search

The site-specific N-glycoproteomic experiment was performed as previously described.[60] Briefly, sgNT and sgSPPL3 221 cells were TMT labeled along with 4 other unrelated samples. Two TMT6 labeling sets were performed as biological replicates. 221 cells expressing sgNT in PBS were used as the reference control channel. Log2-median strategy was used for each sample channel followed by comparing to the reference channel. For sample processing, cell pellets were lysed in the lysis buffer containing 4% SDS (w/v), 50 mM HEPES, pH 8.0 and sonicated for 20 min (30 s on, 30 s off) using Bioruptor at 4°C. After centrifugation at 14,000 × g for 15 min, the supernatants were collected, and the protein amounts were measured using Pierce BCA Protein Assay Kit (Thermo Scientific). 400 μg protein from each sample was reduced and alkylated with 10 mM TCEP (0.5 M stock, Thermo Scientific) and 20 mM IAM at 37°C for 60 min in the dark. A mixture of Sera-Mag SpeedBeads (GE Healthcare, cat.no. 45152101010250; cat.no. 65152105050250) was rinsed twice with water and then added to protein lysates at the working ratio of 10:1 (w/w, beads to proteins). After adding acetonitrile (ACN) to a final percentage of 70% (v/v), the beads and proteins were incubated for 10 min at room temperature off the rack, followed by resting on magnetic rack for 2 min to remove the supernatant. The beads were washed three times with 90% (v/v) ACN, resuspended in 50 mM HEPES (pH 8.0) containing sequencing grade modified trypsin (1:40 of enzyme-to-protein ratio), and incubated at 37°C overnight in a ThermoMixer with mixing at 1000 rpm. The resulting digested peptides in the supernatant were collected, followed by labeling with TMTsixplex isobaric label Reagents according to the manufacturer's instruction (Thermo Scientific).

The dried TMT-labeled peptides were redissolved in loading buffer (80% (v/v) ACN and 1% TFA) and loaded five times to spin-columns self-packed with the Ultimate Hydrophilic Interaction Liquid Chromatography (HILIC) Amphion II beads (5 μm, Welch, Lot. no. 7301.26). After three washes with washing buffer (75% (v/v) ACN, 1% TFA), the retained TMT-labeled glycopeptides were eluted with 100 μL 0.1% TFA twice and dried in a SpeedVac concentrator. Subsequently, basic reverse phase fractionation for enriched glycopeptides was performed on an Agilent 1100 series high-performance liquid chromatography (HPLC) system installed with a XBridge C18 column (3.5 μm particles, 1.0 mm × 150 mm, Waters). Peptides were collected in a time-based mode from 6 to 64 min and pooled into 6 concatenated fractions.

LC-MS analysis was performed on an Orbitrap Fusion Lumos Tribrid Mass Spectrometer (Thermo Scientific) coupled to a Dionex UltiMate 3000 UHPLC system (Thermo Scientific). The MS instrument settings were described briefly in the following. MS1 settings: Orbitrap Resolution-120 k, Mass Range (m/z)-350-2000, Maximum IT-50 ms, AGC target-5e5, RF Lens-60%, Precursor selection range (m/z)-700-2000; MS2 settings: Isolation window-2 m/z, Scan range mode-define first mass-132, Activation type-HCD, Collision energy-25, Detector type-Orbitrap, Orbitrap resolution-15 K, Maximum IT-150 ms, AGC target-5e5; MS3 settings: Precursor selection range-700-2000, Number of Notches-10, First mass (m/z)-120, Activation type-HCD, Collision energy (%)-35, Detector type-Orbitrap, Orbitrap resolution-15 K, Maximum IT-350 ms, AGC target-5e5, Number of Dependent Scans-10.

All raw files were processed by GlycoBinder.[60] Main parameters used for GlycoBinder include fully specific trypsin digestion with maximal two missed cleavage and mass tolerance for precursors and fragment ions of 10 and 20 ppm, respectively. Cysteine carbamidomethylation and TMT6 on peptide N-termini and lysine residues were set as fixed modifications and methionine oxidation was set as a variable modification. The reviewed human protein database was downloaded from Swiss-Prot (October 2020, human, 20,370 entries). GlycoBinder propagates all glycopeptide-to spectra matches and directly reported the quantification of glycosylation sites, glycan compositions, and intact glycopeptides in separate txt files.

All identified N-glycopeptides and their glycan compositions were classified into 6 glycan types based on the number of different monosaccharide moieties, including hexose (Hex), N-acetylhexosamine (HexNAc), N-acetylneuraminic acid (Neu5Ac), and fucose (Fuc). "Complex" type corresponds to the glycan composition of HexNAc (≥4)-Hex(≥3)-NeuAc(any)-Fuc(any). "A4/A3B" represents 4 potential number of branches or 3 branches with a bisect, corresponding to the glycan composition of HexNAc (≥6)-Hex(≥3)-NeuAc(any)-Fuc(any).

Glycomics analysis

The cells were lysed in 50 mM ammonium bicarbonate buffer, followed by treatment with 25 mM DTT, and incubated at 50°C for 30 min. The samples were then desalted by centrifugal filtration (Amicon filters, MilliporeSigma) and ultrasonicated to dissolve the desalted protein. Glycomics analysis was performed as previously described.[61] Briefly, protein from cell lysate was treated with

PNGase F (New England Biolabs) at 37°C for 48 h to release glycans. The released *N*-glycans were recovered with 10 kDa Amicon centrifuge filters (MilliporeSigma). Glycans were permethylated using methyl iodide in the presence of NaOH-DMSO. The permethylated glycans were extracted with dichloromethane and dried under nitrogen air. Glycan samples were dissolved in methanol, mixed with 2,5-dihydroxybenzoic acid (2,5-DHB) in the ratio 1:1, and analyzed in the positive ion mode by MALDI TOF/TOF-MS (AB SCIEX MALDI TOF/TOF 5800, Applied Biosystem MDS Analytical Technologies).

QUANTIFICATION AND STATISTICAL ANALYSIS

All statistical analyses were performed using the Prism GraphPad Software. Two group comparisons were analyzed using a two-tailed paired t test, multiple group comparisons were analyzed using a one-way ANOVA. The standard error of the mean (SEM) was calculated for all experiments and displayed as errors bars in graphs. Statistical details for each experiment are described in figure legends.